

Crystallization behavior of iron- and boron-containing nepheline ($\text{Na}_2\text{O} \cdot \text{Al}_2\text{O}_3 \cdot 2\text{SiO}_2$) based model high-level nuclear waste glasses

DESHKAR, Ambar, AHMADZADEH, Mostafa, SCRIMSHIRE, Alex <<http://orcid.org/0000-0002-6828-3620>>, HAN, Edmund, BINGHAM, Paul <<http://orcid.org/0000-0001-6017-0798>>, GUILLEN, Donna <<http://orcid.org/0000-0002-7718-4608>>, MCCLOY, John <<http://orcid.org/0000-0001-7476-7771>> and GOEL, Ashutosh <<http://orcid.org/0000-0003-0139-9503>>

Available from Sheffield Hallam University Research Archive (SHURA) at:

<http://shura.shu.ac.uk/22031/>

This document is the author deposited version. You are advised to consult the publisher's version if you wish to cite from it.

Published version

DESHKAR, Ambar, AHMADZADEH, Mostafa, SCRIMSHIRE, Alex, HAN, Edmund, BINGHAM, Paul, GUILLEN, Donna, MCCLOY, John and GOEL, Ashutosh (2018). Crystallization behavior of iron- and boron-containing nepheline ($\text{Na}_2\text{O} \cdot \text{Al}_2\text{O}_3 \cdot 2\text{SiO}_2$) based model high-level nuclear waste glasses. *Journal of the American Ceramic Society*, 102 (3), 1101-1121.

Copyright and re-use policy

See <http://shura.shu.ac.uk/information.html>

DR PAUL A BINGHAM (Orcid ID : 0000-0001-6017-0798)

DR DONNA P GUILLEN (Orcid ID : 0000-0002-7718-4608)

DR JOHN MCCLOY (Orcid ID : 0000-0001-7476-7771)

DR ASHUTOSH GOEL (Orcid ID : 0000-0003-0139-9503)

Article type : Article

Corresponding author mail id : ashutosh.goel@rutgers.edu

Contributing editor: Eric Vance

**Crystallization behavior of iron- and boron-containing nepheline
(Na₂O•Al₂O₃•2SiO₂) based glasses: Implications on the chemical
durability of high-level nuclear waste glasses**

Ambar Deshkar,¹ Mostafa Ahmadzadeh,² Alex Scrimshire³, Edmund Han,¹ Paul
A. Bingham³, Donna Guillen⁴, John McCloy,² Ashutosh Goel^{1,1}

¹Department of Materials Science and Engineering, Rutgers-The State University of New
Jersey, Piscataway, NJ, USA

²School of Mechanical & Materials Engineering and Materials Science & Engineering
Program, Washington State University, Pullman, WA, USA

³Materials and Engineering Research Institute, Sheffield Hallam University, Sheffield, South
Yorkshire, United Kingdom

¹ Corresponding author: Email: ag1179@soe.rutgers.edu; Ph: +1-848-445-4512

This article has been accepted for publication and undergone full peer review but has not
been through the copyediting, typesetting, pagination and proofreading process, which may
lead to differences between this version and the Version of Record. Please cite this article as
doi: 10.1111/jace.15936

This article is protected by copyright. All rights reserved.

⁴Materials Science and Engineering Department, Idaho National Laboratory, Idaho Falls, ID,
United States

Abstract

The present study focuses on understanding the relationship between iron redox, composition, and heat-treatment atmosphere in nepheline-based model high-level nuclear waste glasses. Glasses in the $\text{Na}_2\text{O}-\text{Al}_2\text{O}_3-\text{B}_2\text{O}_3-\text{Fe}_2\text{O}_3-\text{SiO}_2$ system with varying $\text{Al}_2\text{O}_3/\text{Fe}_2\text{O}_3$ and $\text{Na}_2\text{O}/\text{Fe}_2\text{O}_3$ ratios have been synthesized by melt-quench technique and studied for their crystallization behavior in different heating atmospheres – air, inert (N_2) and reducing ($96\%\text{N}_2-4\%\text{H}_2$). The compositional dependence of iron redox chemistry in glasses and the impact of heating environment and crystallization on iron coordination in glass-ceramics have been investigated by Mössbauer spectroscopy and vibrating sample magnetometer (VSM). While iron coordination in glasses and glass-ceramics changed as a function of glass chemistry, the heating atmosphere during crystallization exhibited minimal effect on iron redox. The change in heating atmosphere did not affect the phase assemblage but did affect the microstructural evolution. While glass-ceramics produced as a result of heat treatment in air and N_2 atmospheres developed a golden/brown colored iron-rich layer on their surface, those produced in a reducing atmosphere did not exhibit any such phenomenon. Further, while this iron-rich layer was observed in glass-ceramics with varying $\text{Al}_2\text{O}_3/\text{Fe}_2\text{O}_3$ ratio, it was absent from glass-ceramics with varying $\text{Na}_2\text{O}/\text{Fe}_2\text{O}_3$ ratio. An explanation of these results has been provided on the basis of kinetics of diffusion of oxygen and network modifiers in the glasses under different thermodynamic conditions. The plausible implications of the formation of iron-rich layer on the surface of glass-ceramics on the chemical durability of high-level nuclear waste glasses have been discussed.

1. Introduction

Nepheline is a feldspathoid that occurs in nature in low silica-content intrusive and volcanic rocks with an ideal composition $\text{Na}_3\text{KAl}_4\text{Si}_4\text{O}_{16}$. Its crystal structure is a stuffed derivative of tridymite (SiO_2), a hexagonal system where half of the Si tetrahedral atoms are replaced by Al atoms, and a $P6_3$ space group symmetry with Na^+ , K^+ cations “stuffed” within the channels in the six-membered rings made up of the TO_4 (T=Si, Al) tetrahedra.^{1, 2} Glasses with stoichiometric pure Na nepheline composition ($\text{Na}_2\text{O}\cdot\text{Al}_2\text{O}_3\cdot 2\text{SiO}_2$) exhibit a structural resemblance to vitreous SiO_2 since its meta-aluminous nature – i.e. $\text{Na}/\text{Al}=1$ – means that all the AlO_4^- tetrahedra are fully charge compensated by Na^+ making the network fully polymerized.³

Crystallization in nepheline-based glasses occurs through a sequence of polymorphic transformations which strongly depends on their compositional chemistry. A glass derived from the stoichiometric nepheline ($\text{Na}_2\text{O}\cdot\text{Al}_2\text{O}_3\cdot 2\text{SiO}_2$) composition crystallizes predominantly at the surface via formation of low-carnegieite, which is an orthorhombic polymorph of NaAlSiO_4 .⁴ Being a metastable phase, low-carnegieite transforms into hexagonal nepheline with time as temperature is increased. On further heating to 1400 °C, nepheline transforms into the high temperature (high-T) cubic carnegieite, the stable polymorph of NaAlSiO_4 at that temperature.⁵ However, crystallization in SiO_2 -deficient (or Al_2O_3 -rich) nepheline-derived glasses has been shown to initiate from cubic carnegieite which may or may not transform into hexagonal nepheline depending on compositional complexity.^{6, 7}

Several cations, such as Mg^{2+} , Ca^{2+} , Fe^{2+} , Fe^{3+} , Mn^{2+} , or Ti^{4+} , are known to incorporate into the crystal structure of natural and synthetic nephelines.^{2, 8} The interaction of these cations with framework and non-framework cations in the aluminosilicate network results in interesting properties due to which nepheline-based glasses and glass-ceramics have found wide-ranging technological applications. For example, dopants such as TiO_2 , Fe_2O_3 , and Nb_2O_5 have been used as nucleation agents for obtaining controlled uniform growth of nepheline crystals in the bulk of glasses.^{4, 6, 9} Strengthened glass-ceramics have been obtained by application of surface compression through either $\text{K}^+ \leftrightarrow \text{Na}^+$ ion exchange treatment,⁶ or through surface glazing with low thermal expansion glasses. These nepheline glass-ceramics have found commercial use as dental porcelain,^{10, 11} tableware,¹² and more recently, as colored opaque glass-ceramics by doping transition metals such as Fe_2O_3 and lanthanide oxides into nepheline, applicable for electronic packaging and casings.^{13, 14} On the other hand, crystallization of nepheline in high-level radioactive waste (HLW) glasses is highly detrimental to the chemical durability of the glassy waste forms, and dedicated efforts are being made to design HLW glass compositions with minimal tendency towards nepheline crystallization.^{15, 16, 17} Therefore, from a radioactive waste vitrification perspective, it is of utmost importance to understand the compositional and structural drivers controlling the nucleation and crystallization in nepheline-based glass systems.

The present study is focused on understanding the role of the redox chemistry of iron in the crystallization behavior of nepheline based glasses in the $\text{Na}_2\text{O} - \text{Al}_2\text{O}_3 - \text{B}_2\text{O}_3 - \text{Fe}_2\text{O}_3 - \text{SiO}_2$ system. The problem lies in the fact that iron oxides / nitrates are an integral component of sodium- and aluminum-rich HLW stored in underground tanks at the Hanford site in Washington State.¹⁸ In general, typical Hanford HLW glasses contain 2 – 10 wt.% Fe_2O_3 with a mean concentration of ~7 wt%.¹⁹ During HLW vitrification into borosilicate glass

matrices, the presence of iron in the melt results in two major challenges for the processing and development of final waste forms. In the first case, iron interacts with other transition metal cations (for example, Ni^{2+} , Mn^{2+} , Cr^{3+}) in the glass melter to form spinels (for example, NiFe_2O_4). The formation of spinel crystals in the glass melter is problematic, because large insoluble crystals can settle on the floor of the melter and partially or completely block the discharge throat and riser.^{20,21} In the second scenario, the as-formed spinel crystals tend to act as nucleation sites for the crystallization of nepheline during cooling of HLW glass in canisters, which results in a waste form with poor chemical durability.^{4, 17, 22} In our recent studies,^{4, 23} we have shown that iron forms a solid solution with nepheline crystallized from $\text{NaAl}_{(1-x)}\text{Fe}_x\text{SiO}_4$ glass, with a level of incorporation up to $x = 0.37$, and promotes the crystallization of nepheline over carnegieite. Given the strong interaction of iron with nepheline, it is imperative to understand the chemistry of iron in HLW glasses, and its implications for crystallization behavior.

It has long been known that the structural role played by iron in silicate glasses is dictated principally by redox chemistry governing the relative proportions of ferrous and ferric ions in glass melts involving oxygen. Therefore, the redox ratio of iron also affects the silicate melt structure. Fe^{2+} and Fe^{3+} play different roles in the glass network, and their relative proportions are dependent on a variety of factors, including melt composition, oxygen fugacity, temperature, pressure, and total iron content.^{24, 25} When in the Fe^{3+} state, iron acts as a network former in silicate frameworks as it prefers to be tetrahedrally coordinated by forming FeO_4^- , which then requires charge compensation by an alkali or alkaline-earth cation.^{24, 25, 26, 27} According to Mysen,²⁵ the redox relations and hyperfine parameters of Fe^{3+} and Fe^{2+} are not dependent on the nature of Fe^{3+} - charge balancing cations of the iron oxide dissolved in glasses and melts. Therefore, it is highly likely that for Fe^{3+} predominantly in

Accepted Article

tetrahedral coordination, some of the alkali or alkaline-earth cations that charge balance Al^{3+} in aluminosilicate glasses may be transferred to Fe^{3+} , or Fe^{3+} in 4-fold coordination may form some complex with Fe^{2+} as has been proposed by Virgo and Mysen²⁸ and Kress and Carmichael.²⁹ Thus, there is no evidence that specific alkalis or alkaline-earth cations may exhibit a preference for charge balance of Fe^{3+} in tetrahedral coordination in an aluminosilicate glass. In some aluminosilicate glasses, the $\text{Fe}^{3+}/\Sigma\text{Fe}$ redox ratio has been shown to be positively correlated with increasing total iron content and with decreasing ionization potential of the alkali and alkaline-earth cation.^{4, 25} It differs from Al^{3+} , however, in that Fe^{3+} can also be an octahedral network modifier, even when other cations could provide charge compensation for tetrahedral coordination.²⁴ The structural role of Fe^{2+} in silicate glasses, on the other hand, is still debated. While some studies have reported Fe^{2+} to exist in 4- and 5- fold coordination in alkaline-earth silicate glasses,^{30, 31} others have reported it to exist in 6-coordination and behave as network modifier.^{32, 33} In meta-aluminous silicate glasses, Fe^{2+} has been shown to exist in a range of coordination numbers, from something resembling 4 in the Fe-bearing $\text{NaAlSi}_2\text{O}_6$ system to 5- or 6-fold coordination in alkaline-earth aluminosilicates ($\text{Ca}_{0.5}\text{AlSi}_2\text{O}_6$ or $\text{Mg}_{0.5}\text{AlSi}_2\text{O}_6$).²⁵ In borosilicate glasses, ferrous ions have been reported to exist mainly in 5 and 6-fold coordination.²⁷ According to Cochain et al.²⁷ there exists a subtle interplay between Fe^{3+} and the other tetrahedrally coordinated cations (Si, B) in borosilicate glass structures with changing iron redox chemistry because of the competition between tetrahedral Fe^{3+} and B^{3+} for charge compensation by alkali/alkaline-earth cations.²⁷

With this perspective, the compositional and structural complexity presented by an iron-containing aluminoborosilicate glass system makes it highly interesting to study the mechanisms that govern its crystallization behavior. Accordingly, an iron-free glass with

composition 25 Na₂O – 20 Al₂O₃ – 10 B₂O₃ – 45 SiO₂ (mol.%) designed in the primary crystallization field of nepheline (and its polymorphs) has been chosen as the baseline³⁴. The composition is per-alkaline and has been designed to make it similar to typical US HLW glass compositions. The chosen baseline composition is expected to be homogeneous (no phase separation) based on a criteria reported by Qian et. al.³⁵ for aluminoborosilicate glasses where the ratio of their excess alkali content, Na₂O_{ex} ([Na₂O]-[Al₂O₃]) – to – [B₂O₃], i.e. [Na₂O_{ex}]/[B₂O₃] decides their homogeneity. Based on this criteria, alkali aluminoborosilicate glasses with [Na₂O_{ex}]/[B₂O₃] > 0.5 have minimal tendency towards phase separation. This criterion has been discussed in detail in our recent publication.³⁶ An attempt has been made to synthesize glasses by partially substituting Fe₂O₃ for all the four components in the baseline glass, i.e. Na₂O/Fe₂O₃, Al₂O₃/Fe₂O₃, B₂O₃/Fe₂O₃, SiO₂/Fe₂O₃. The redox chemistry of iron in as synthesized glasses and its impact on their crystallization behavior as a function of heat treatment atmosphere – air/inert/reducing – has been investigated.

2. Experimental Procedures

2.1 Glass synthesis

Glasses with varying Al₂O₃/Fe₂O₃ (labeled as AF-*x*), B₂O₃/Fe₂O₃ (labeled as BF-*x*) and Na₂O/Fe₂O₃ ratios (labeled as NF-*x*), where *x* represents the batched Fe₂O₃ content in mol.%, were synthesized using the melt-quench technique. The iron-free baseline glass is designated as AF-0. The homogeneous mixtures of batches (corresponding to 70 g oxide glass), comprising SiO₂ (Alfa Aesar; >99.5%), Na₂SiO₃ (Alfa Aesar; anhydrous, tech.), Al₂O₃ (ACROS Organics; extra pure; 99%), H₃BO₃ (ACROS Organics; extra pure, 99+%), and Fe₂O₃ (Sigma Aldrich; ≥99%), were melted in 90%Pt–10%Rh crucibles in an electric furnace at 1650 °C for 2 h (owing to their high Al₂O₃ content). The melts were quenched on copper plate followed by annealing at 410 °C for 1 h and then slowly cooling to room temperature.

The annealing temperature was determined from the estimated value of glass transition temperature (T_g) using SciGlass database, as $T_g - 50$ °C. The samples were analyzed using X-ray diffraction (XRD) to verify that they were amorphous (PANalytical – X’Pert Pro; Cu K_{α} radiation; 2θ range: 10° – 90° ; step size: 0.0065° s^{-1}). The experimental composition of glasses was analyzed by inductively coupled plasma – optical emission spectroscopy (ICP-OES; PerkinElmer Optima 7300V) and flame emission spectroscopy (for sodium; PerkinElmer Flame Emission Analyst 200). Table 1 presents the batched and experimental compositions of the studied glasses.

2.2 Non-isothermal crystalline phase evolution in glasses

The glasses were crushed to produce coarse glass grains in the particle size range of 0.85 to 1 mm. Differential scanning calorimetry (DSC) data were collected using a Simultaneous Thermal Analyzer (Perkin Elmer STA 8000) in the temperature range of 30 °C – 1580 °C at a heating rate (β) of 10 °C min^{-1} under a constant flow of nitrogen gas. The temperatures, corresponding to onset of glass transition (T_g), onset (T_c) and peak (T_p) of crystallization, and melting (T_m), were obtained from DSC scans. The DSC data reported for any glass composition are the average of at least three thermal scans.

To understand the non-isothermal crystalline phase evolution in glasses as a function of glass composition, glass pieces (~2-3 gram) were heated (in Al_2O_3 crucibles) to different temperatures (Carbolite BLF 1800 furnace) in the crystallization region (per DSC data) at 10 °C min^{-1} and were air quenched as soon as the desired temperatures were reached. All the heat-treated samples were characterized qualitatively by powder XRD (PANalytical – X’Pert Pro; Cu $K_{\alpha 1}$ radiation).

2.3 Isothermal crystalline phase evolution in glasses

The crystalline phase evolution in the glasses under isothermal conditions was studied by heating the glasses (except the baseline glass, BL) at 700 °C for 1 hour ($\beta = 10^\circ\text{C min}^{-1}$) in a tube furnace (GSL-1500X-RTP50; MTI Corporation, CA) in air, N₂ (inert) and N₂-H₂ (reducing; 4% H₂ - 96% N₂) environments, respectively. The isothermal heat treatment temperature (700 °C) was chosen on the basis of results obtained from DSC data and non-isothermal crystallization experiments (as explained in Section 2.2). The heat-treated glass samples were allowed to cool to room temperature in the furnace by natural cooling. The resulting glass-ceramics were divided in two parts. The first part of the sample was crushed to powder with particle size < 45 μm and mixed with 10 wt.% Al₂O₃ as internal standard for quantitative crystalline phase analysis by XRD using the Rietveld analysis method (PANalytical Highscore). XRD used was PANalytical X'Pert Pro XRD with a Cu-K α tube 45 kV and 40 mA in the 2 θ range of 10 – 90° with 0.002° 2 θ step size and dwell time of 5.7 s. The second part of the glass-ceramic sample was chemically etched using 2 vol.% HF solution for 1 min to remove the glassy phase from the sample surface. Microstructural observations were performed on unpolished samples using a field emission – scanning electron microscopy (SEM; ZEISS Sigma FE-SEM) being operated in secondary electron imaging mode. The elemental distribution mapping was performed by energy dispersive spectroscopy (EDS; X-Max Oxford Instruments; Aztec software).

2.4 Mössbauer Spectroscopy

Mössbauer spectroscopy was performed to understand the impact of glass composition and crystallization atmosphere on the redox chemistry of iron in glasses and resultant glass-ceramics. Accordingly, Mössbauer spectroscopy was carried out at 20 °C on glasses and glass-ceramics (produced after isothermal heat treatment at 700 °C, for 1 hr in air, N₂ or

96%N₂-4%H₂ environments) using a constant acceleration spectrometer with a 25 mCi ⁵⁷Co source in a Rh matrix. Absorbers were prepared from finely ground samples that were mixed with graphite powder, and then ground further, to ensure a Mössbauer thickness $t < 1$.² Spectra were measured in the velocity range ± 12 mm s⁻¹ relative to α -Fe and were fitted using the Recoil analysis software package. For the amorphous glass samples, two broadened Lorentzian paramagnetic doublets were fitted to the resulting Mössbauer spectra. For the glass-ceramic samples, two broadened Lorentzian doublets and two sextets were fitted to each spectrum. When fitting all spectra, it was assumed that the recoil-free fraction ratio $f(\text{Fe}^{3+})/f(\text{Fe}^{2+}) = 1.0$.

2.5 Magnetic measurements of glass-ceramics

Magnetic measurements, owing to their non-destructive nature and high sensitivity towards iron-containing phases, are a rapid characterization technique to obtain valuable information about distribution of Fe in different phases present in the sample.²³ Therefore, magnetic measurements were performed on isothermally produced glass-ceramics using a vibrating sample magnetometer (VSM, PMC3900, Lakeshore Cryotronics, Westerville, OH). Magnetic hysteresis loops of the samples isothermally heat-treated in different environment were collected at maximum applied field of 1.8 T using field increments of 2 mT. The first order reversal curves (FORCs)³⁷ data of the same samples were also obtained with a field increment of 6 mT, and processed employing FORCinel software (V2.05 in IGOR Pro6, WaveMetrics, Portland, OR).³⁸

² Mossbauer thickness is the effective thickness of a source (t_s) or absorber (t_a). For an experiment involving element Z, Mossbauer thickness (t) is given by $t = n\sigma af$, where n is the number of atoms of Z per cm², σ is the cross section for resonance absorption, a is the fractional abundance of the Z nuclide which show the Mossbauer effect being observed, and f is the recoil-free fraction.

3. Results

3.1 Glass forming ability

The iron-free baseline glass (AF-0) was obtained by pouring the melt on a copper plate. This resulted in a transparent, homogeneous glass with an amorphous structure confirmed by XRD. However, incorporation of Fe_2O_3 led to a decrease in the glass-forming ability of the melts. We were able to obtain amorphous samples with Fe_2O_3 content varying between 0 – 5 mol.% in a system with varying $\text{Al}_2\text{O}_3/\text{Fe}_2\text{O}_3$ ratio (AF series), while in compositions with varying $\text{Na}_2\text{O}/\text{Fe}_2\text{O}_3$ ratio (NF series), we could only obtain a glass with a Fe_2O_3 content of 2.5 mol.%. Figure S1 presents the XRD patterns of the amorphous samples. The compositional analysis of the as synthesized glasses revealed volatility of Na_2O and B_2O_3 from the glass melts in the range of 2 – 5% and 12 – 15%, respectively. An increase in Fe_2O_3 content to 6.25 mol.% in AF glasses or to 5 mol.% in NF glasses resulted in crystallization of magnetite phase (Fe_3O_4 ; cubic; PDF# 98-002-0596) (as shown in Figure S2) even after re-melting the samples twice followed by quenching the melt in cold water (Figure S2 shows results of water-quenched trials). Furthermore, substitution of Fe_2O_3 for B_2O_3 (labeled as BF-2.5) was also attempted but a 2.5 mol.% substitution, in this case, led to crystallization of low-carnegieite (NaAlSiO_4 ; orthorhombic; PDF# 98-007-3511) with minor quantities of quartz (SiO_2 ; hexagonal; PDF# 97-004-1474) and magnetite phases (Fe_3O_4 ; cubic; PDF# 98-002-0596) as shown in Figure S2. Hence, only four compositions, namely, AF-0, AF-2.5, AF-5 and NF-2.5, were considered for further studies.

3.2 Mössbauer Spectroscopy of glasses

Figure 1 presents the fitted Mössbauer spectra of all the iron-containing glasses. The fitted hyperfine parameters for the studied glasses show the presence of Fe^{2+} and Fe^{3+} components. The fitted center shift (CS), quadrupole splitting (QS) and line width (LW)

parameters shown in Table 2 are consistent with the view that Doublet DD1 represents tetrahedrally-coordinated Fe^{3+} and Doublet D2 represents Fe^{2+} ions octahedral sites, with some tetrahedral and possibly 5-coordinated sites also occupied.^{25, 27, 28, 39, 40, 41} The ratio of the area of Doublet 1 to the total spectral area can thus be taken to provide the $\text{Fe}^{3+}/\Sigma\text{Fe}$ redox ratio, assuming that the recoil-free fraction ratio $f(\text{Fe}^{3+})/f(\text{Fe}^{2+}) = 1.0$ in these glasses. The Mössbauer results reveal an increase in $\text{Fe}^{3+}/\Sigma\text{Fe}$ ratio with increasing $\text{Fe}_2\text{O}_3/\text{Al}_2\text{O}_3$ concentration in the AF glass series. The redox ratio of iron in aluminosilicate glasses, $\text{Fe}^{3+}/\Sigma\text{Fe}$, is known to be a positive function of the total iron concentration in glass and inversely proportional to the ionic field strength of the cation serving to charge balance Al^{3+} in tetrahedral coordination.²⁵

When comparing glasses with constant Fe_2O_3 content, the glass NF-2.5 has a lower $\text{Fe}^{3+}/\Sigma\text{Fe}$ ratio than glass AF-2.5. This behavior may be explained on the basis of either lower optical basicity (OB) of glass NF-2.5 (0.585) in comparison to AF-2.5 (0.590), or lower availability of Na^+ to charge compensate FeO_4^- units in NF-2.5 as has been discussed below.

In terms of basicity of glass melts, it is well known that there exists an empirical relationship between optical basicity and redox chemistry of iron in oxide glasses wherein increasing basicity favors the upper oxidation state in $\text{Fe}^{2+} - \text{Fe}^{3+}$ redox couple.⁴² According to Duffy,⁴² this occurs through donation of negative charge by the oxygen atoms surrounding the metal ion. Increasing the basicity of glass leads to a greater degree of negative charge on the constituent oxygen atoms and hence, to a greater ‘electron donor power’. While generally acceptable, this relationship may not be true in all the cases. For example, as has been shown by Schreiber et al.,⁴³ in a series of sodium silicate glasses containing 1 wt.% Fe_2O_3 , the $\text{Fe}^{3+} - \text{Fe}^{2+}$ couple becomes more reduced as the composition becomes more basic with increasing

Na/Si ratio up to about unity ($\text{Na/Si} = 1$) and after that point the redox couple becomes more oxidized as the composition becomes even more basic. This implies that the actual dependence of individual redox couples should not be generalized, as it is a function of the availability of solvation sites for the redox states of the multivalent element in the melt structure.⁴³

From a structural viewpoint, while it is well known that tetrahedral aluminum is preferentially charge compensated by alkali cations, an ambiguity still exists in literature over preferential compensation of BO_4 vs. FeO_4 units.^{27, 46} In the case of iron-free baseline AF-0 glass, ideally 20 mol.% Na_2O will be consumed to charge compensate four-fold aluminum, while the remaining 5 mol.% (i.e., excess Na_2O hereafter referred as $\text{Na}_2\text{O}_{\text{ex}}$) will act as charge compensator for BO_4 units. Therefore, we can expect boron to be present in both trigonal (BO_3) and tetrahedral (BO_4^-) coordination in this glass. For the glass AF-2.5, the aluminum coordination is unlikely to change, as there are sufficient alkali cations to charge compensate tetrahedral aluminum units. With respect to the coordination of boron and iron, since Mössbauer spectroscopy reveals iron to be present in both 2+ and 3+ oxidation states, we expect slightly higher concentration of BO_4 units in this glass (compared to glass AF-0) due to higher availability of Na^+ for charge compensation (considering that all the Fe^{3+} is in tetrahedral coordination, and both FeO_4^- and BO_4^- have equal affinity to attract Na^+ for charge compensation). On the other hand, in glass NF-2.5, the concentration of $\text{Na}_2\text{O}_{\text{ex}}$ is 2.5 mol.% (remaining after charge compensation of AlO_4 units). This will result in a greater competition between FeO_4 and BO_4 units for charge compensation by Na^+ . Since Mössbauer spectroscopy demonstrates lower $\text{Fe}^{3+}/\Sigma\text{Fe}$ ratio in this glass (when compared to glass AF-2.5), this indirectly implies preferential charge compensation of BO_4^- units over FeO_4^- . However,

detailed structural studies, for example, boron K-edge XANES spectroscopy, need to be performed in order to strengthen this hypothesis.

Here, it should be noted that it is likely that the values obtained for $\text{Fe}^{3+}/\Sigma\text{Fe}$ ratios from ^{57}Fe Mössbauer spectroscopy at 20 °C in the present study may have been overestimated due to paramagnetic hyperfine splitting (hfs) as has been reported in the literature.^{28, 39, 47} For example, comparing the Mössbauer measurements at liquid nitrogen atmosphere (77 K) versus room temperature (298 K), Virgo and Mysen²⁸ demonstrated that the $\text{Fe}^{3+}/\Sigma\text{Fe}$ ratio can be overestimated by about 5% (relative) at higher temperature. However, there also exists literature⁴⁸ where no such effect of temperature on iron redox has been observed. These somewhat conflicting data, nevertheless, suggest that there may be a small effect of glass composition on the ratio of recoil-free fractions of Fe^{3+} and Fe^{2+} . Based on the trends observed in our previous study on iron redox measurements using wet chemistry techniques⁴ and literature,²⁴ it is reasonable to expect the Mössbauer determined $\text{Fe}^{3+}/\Sigma\text{Fe}$ ratio to be accurate, within the stated uncertainties.

3.3 Glass transition and crystallization behavior of glasses

3.3.1 Compositional and structural dependence of glass transition

Figure 2 shows the DSC scans of all four glasses investigated in the present study, while Table 3 summarizes different transformation temperatures obtained from these scans. The glass transition temperatures (T_g) of the studied glasses were obtained from the onset of the endothermic dip. While we were able to obtain the T_g values for glasses AF-0, AF-2.5 and AF-5, it was difficult to obtain the T_g value for glass NF-2.5 from the DSC scans. The T_g values were observed to decrease upon substitution of Al_2O_3 with Fe_2O_3 , suggesting depolymerization or weakening of the aluminosilicate glass network. Considering that a large

part of the Fe^{3+} ions in the studied glasses are acting as network formers, while a small fraction of Fe^{3+} (possibly) and the majority of the Fe^{2+} ions are network modifiers,^{24, 25, 26} the incorporation of iron in the studied glass samples is likely to generate non-bridging oxygens (NBOs) leading to depolymerization of the glass network. The generation of NBOs in silicate glass network due to addition of Fe_2O_3 has been previously reported in literature,⁴⁹ including in our previous study on a similar subject.⁴ Further, any $\text{Si}^{\text{IV}} - \text{O} - \text{Fe}^{\text{IV}}$ linkages formed in the glass (due to the network forming role of Fe^{3+}) will be weaker than $\text{Si}^{\text{IV}} - \text{O} - \text{Si}^{\text{IV}}$ and $\text{Si}^{\text{IV}} - \text{O} - \text{Al}^{\text{IV}}$ linkages, due to the lower bond energy of $\text{Fe}-\text{O}$ (407 kJ mol^{-1}) in comparison to $\text{Al}-\text{O}$ ($501.9 \text{ kJ mol}^{-1}$) and $\text{Si}-\text{O}$ ($799.6 \text{ kJ mol}^{-1}$).⁵⁰ Consequently, the three-dimensional structure of glass is weakened, resulting in a lower T_g . This argument is also supported by the results of Klein et al.,⁵¹ where it has been shown that the incorporation of iron in an aluminosilicate glass network reduces its viscosity. It should be noted here that since the ferric ion (Fe^{3+}) has higher charge and a lower ionic radius than the ferrous ion (Fe^{2+}), this leads to a larger effective charge (charge per surface area) of the ferric ion. As a consequence of this attraction, the binding energy between Fe^{3+} and O^{2-} should be higher than that between Fe^{2+} and O^{2-} .^{52, 53} Therefore, even if we account for the presence of both $\text{Fe}^{2+}-\text{O}$ and $\text{Fe}^{3+}-\text{O}$ bonds in the glass structure, the overall three-dimensional network will be weakened.

3.3.2 Impact of composition on non-isothermal crystallization behavior of glasses

With reference to non-isothermal crystallization behavior of glasses, a broad exothermic curve was observed in the DSC scan of iron-free baseline glass AF-0 (Figure 2(a)) with an onset of crystallization (T_c) at $720 \text{ }^\circ\text{C}$ and a peak temperature of crystallization (T_p) of $770 \text{ }^\circ\text{C}$. Upon substituting 2.5 mol.% Fe_2O_3 for Al_2O_3 (in glass AF-2.5, Figure 2(b)), the crystallization behavior changed significantly as the T_c showed a steep decrease to $615 \text{ }^\circ\text{C}$ followed by two narrow exothermic peaks at $636 \text{ }^\circ\text{C}$ and $671 \text{ }^\circ\text{C}$, as shown in Figure 2(b).

Interestingly, a further increase in Fe_2O_3 content to 5 mol.% in glass AF-5 (Figure 2(c)) increased the T_c to 658 °C, followed by single broad exothermic crystallization peak with its T_p at 713 °C. On the other hand, when 2.5 mol.% of Fe_2O_3 was substituted for equimolar Na_2O (NF-2.5 glass, Figure 2(d)) in the baseline glass, the temperature for onset of crystallization decreased to 613 °C (in comparison to 720 °C for baseline glass, AF-0) along with the presence of two broad exothermic peaks at 641 °C and 733 °C, respectively. The lowering of onset temperature of crystallization with the substitution of Fe_2O_3 for Al_2O_3 or Na_2O may be attributed to the ability of iron to pre-nucleate these glass compositions (as has been shown in our previous study),⁴ thus creating a lower activation energy pathway for crystallization. Further, the presence of a single crystallization exotherm in DSC scans anticipates that the resultant glass-ceramic is formed from a single-phase crystallization or an almost simultaneous precipitation of multiple crystalline phases. On the other hand, the appearance of two crystallization curves points towards the crystallization of at least two phases at well-defined temperatures. The nature of the crystalline phases formed in the glass-ceramic corresponding to the observed crystallization exotherms is discussed below.

The DSC scans of all the investigated glasses exhibit endothermic curves in the temperature range of 870 °C – 1168 °C representing the melting of crystals formed in the glassy matrix. The melting temperature (T_m) of these crystals decreased from 1168 °C to 870 °C with increasing $\text{Fe}_2\text{O}_3/\text{Al}_2\text{O}_3$ molar ratio in glasses, while a decrease in T_m from 1168 °C to 962 °C was observed with substitution of 2.5 mol.% Na_2O by Fe_2O_3 in glass NF-2.5. The T_m value for glass NF-2.5 (962 °C) was considerably higher than its analog glass (AF-2.5; 892 °C) containing an equimolar concentration of Fe_2O_3 .

Figure 3 presents the X-ray diffraction patterns of the air-quenched samples after non-isothermal heat treatments in the crystallization regimen as obtained from DSC data, while Table 4 presents a concise summary of the phase assemblage as a function of glass composition and crystallization temperature. Crystallization in the baseline glass, AF-0, initiated at 840 °C with an unidentified phase followed by the formation of SiO₂-rich non-stoichiometric nepheline (Na_{7.15}Al_{7.2}Si_{8.8}O₃₂, hexagonal; PDF #98-006-5960) as shown in Figure 3(a). No further transformation of nepheline to high temperature cubic carnegieite was observed until 1060 °C. The unidentified phase formed at 840 °C can be either cristobalite (SiO₂; tetragonal; PDF#97-016-2614) or low-carnegieite (NaAlSiO₄; orthorhombic; PDF#98-007-3511). Since the maximum intensity Bragg peaks for both the phases overlap with each other ($2\theta_{\text{max intensity}}$ for cristobalite = 21.312° based on PDF#97-016-2614, and for low-carnegieite = 21.369° and 21.440° based on PDF#98-007-3511), it is difficult to ascertain the formation of one phase over the other based on a single XRD phase reflection as observed in Figure 3(a).

A similar problem was encountered while studying the crystalline phase evolution in glass AF-2.5 (Figure 3(b)), where crystallization initiated at 580 °C with the formation of an unidentified phase, most probably cristobalite or low-carnegieite. An increase in temperature to 600 °C resulted in crystallization of a non-stoichiometric nepheline phase (Na_{7.15}Al_{7.2}Si_{8.8}O₃₂, hexagonal; PDF #98-006-5960) whose intensity increased with an increase in temperature at the expense of the unidentified phase. Further increase in temperature to 640 °C led to the crystallization of magnetite (Fe₃O₄; cubic; PDF#98-002-0596) as a secondary phase from the glassy matrix. By 660 °C, peaks of the unidentified phase had completely disappeared and the crystalline phase assemblage comprised nepheline as the primary phase followed by magnetite as a secondary phase. The crystalline phase

evolution in glass AF-5 followed a pathway similar to glass AF-2.5, where the crystallization initiated with the formation of low-carnegieite (NaAlSiO_4 ; orthorhombic; PDF#98-007-3511) at 600 °C followed by its partial-to-complete transformation to non-stoichiometric nepheline ($\text{Na}_{7.15}\text{Al}_{7.2}\text{Si}_{8.8}\text{O}_{32}$; hexagonal; PDF#98-006-5960) between 640 – 700 °C, along with crystallization of magnetite as the secondary phase (Figure 3(c)).

Crystalline phase evolution in NF-2.5 glass took a different route, as compared to glasses AF-2.5 and AF-5. The crystallinity in this glass initiated at 680 °C with the formation of an unidentified phase that dominates the crystalline phase assemblage until 780 °C, i.e., when the peaks corresponding to non-stoichiometric nepheline ($\text{Na}_{7.15}\text{Al}_{7.2}\text{Si}_{8.8}\text{O}_{32}$, hexagonal, PDF #98-006-5960) were detected. The unidentified crystalline phase is probably dominated by cubic carnegieite (NaAlSiO_4 ; cubic; PDF#98-003-4884), a high temperature polymorph of nepheline, (Figure 3(d)) as Bragg reflections for this phase were matched with the XRD pattern but with slight shifts in 2-theta values. The crystalline phase evolution was significantly slower than with samples AF-2.5 or AF-5, and peaks corresponding to non-stoichiometric nepheline ($\text{Na}_{7.15}\text{Al}_{7.2}\text{Si}_{8.8}\text{O}_{32}$, hexagonal, PDF #98-006-5960) were not detected until 780 °C. Until 840 °C, the XRD patterns showed a gradual increase in non-stoichiometric nepheline, with a dominant presence of an unidentified phase, with magnetite as a minor phase. A gradual increase in temperature to ≥ 800 °C resulted in complete conversion of unidentified phases (probably cubic carnegieite) to non-stoichiometric nepheline ($\text{Na}_{7.15}\text{Al}_{7.2}\text{Si}_{8.8}\text{O}_{32}$; hexagonal; PDF#98-006-5960) along with the formation of magnetite (Fe_3O_4 ; cubic; PDF#98-002-0596) as a secondary phase.

3.3.3 *Impact of composition and heat treatment atmosphere on the isothermal crystalline phase evolution in glass-ceramics*

Figure S3 presents the XRD pattern of glass AF-0 heat-treated at 700 °C for 1 h in air. The crystalline phase assemblage of the resulting glass-ceramic is comprised of ~34 wt.% nepheline and ~10% low-carnegieite with ~56 wt.% residual glassy phase, as shown in Table 5. Some minor phase reflections corresponding to an unidentified secondary phase can also be observed in the XRD pattern. Table 5 also presents the results of quantitative crystalline phase analysis of iron-containing glass-ceramics (isothermal heat treatment 700 °C for 1 h under three different environments – air, N₂ and N₂-H₂) obtained by Rietveld refinement. The crystalline phase assemblage in all the iron-containing glass-ceramics comprised hexagonal nepheline as the primary phase followed by the presence of trace amounts of magnetite and/or hematite crystals. Carnegieite was observed as secondary phase in glass-ceramics in AF-5 and NF-2.5. The most important observation from the results presented in Table 5 is that the crystalline phase assemblage in the studied glass-ceramics is governed by the chemical composition (and structure) of their parent glasses. The heat treatment atmosphere (air vs. inert vs. reducing) does not exhibit a significant impact on the crystalline phase assemblage of the resultant glass-ceramics. When compared with the crystalline phase assemblage of the AF-0 glass-ceramic, it is evident that iron tends to promote crystallization of nepheline over carnegieite as has also been shown in our previous studies.^{4,23} The high amount of residual glassy phase (56% – 75%) in all the glass-ceramics may be attributed to the presence of 10 mol.% B₂O₃ in the studied glass system. In nepheline-based glass-ceramic systems, boron has been shown to be partitioned in the residual glassy phase (instead of being incorporating into aluminosilicate crystal structure) resulting in higher concentration of BO₄ units (in comparison to its parent glass), thus stabilizing the residual glassy phase.^{15, 17, 54, 55}

3.3.4 *Impact of composition and heat treatment atmosphere on the microstructure of glass-ceramics*

While a minimal impact of heat treatment atmosphere was observed on the crystalline phase assemblage of isothermally produced glass-ceramics, the microstructure of these glass-ceramics (as observed under SEM – EDS) revealed a significant impact of heat treatment atmosphere as is evident from SEM images of the interface between the surface and bulk of the samples shown in Figure 4 and S4. From their physical appearance, the glass-ceramics AF-2.5 (Figure S4) and AF-5 showed the presence of crystals both on their surfaces and in volume when heat treated in air and N₂ atmospheres. An approximately 1 – 5 μm thick golden-brown colored layer of crystals was formed on the surface of the glass-ceramics (as its “skin”), while the core of the glass-ceramics still exhibited the brown glassy halo as can be seen in Figure 5. The SEM images of these glass-ceramics exhibit the presence of two distinct microstructures where the crystals on the surface (thin golden layer) exhibit a lath-shaped morphology, while the core is comprised of fine grained crystals (Figure 4(a)). Figure S5 presents an EDS elemental line scan across the interface between surface and bulk of glass-ceramic AF-5 (heat-treated in air) showing the change in iron concentration from surface to bulk of the sample. The EDS elemental mapping of the microstructure reveals that the outer layer of the samples is predominantly rich in iron, while the fine-grained crystals in the core of glass-ceramics are rich in Na, Al and Si (and depleted in iron). This implies that a fraction of the iron acts as a nucleating site for preferential crystallization of nepheline over carnegieite in the volume of the glass, while the remaining iron content partitions out of the glassy matrix (primarily from near the glass surface, as it is the surface that is mainly in contact with the heating atmosphere) and crystallizes as magnetite (Fe₃O₄) and/or hematite (α-Fe₂O₃) on the surface of the glass-ceramic (as analyzed by powder XRD analysis). Further, higher magnification images of glass-ceramics AF-2.5 and AF-5 heat-treated in air

(Figure 6(a) and 6(b)) reveal pseudo-hexagonal rod like structures of nepheline. Tridymite (SiO_2) exhibits similar characteristic microstructure, which suggests that nepheline crystallization in the studied glass system proceeds through a stuffed derivative structure of silica.^{56, 57}

On the other hand, glass-ceramics for compositions AF-2.5 and AF-5 produced in reducing ($\text{N}_2\text{-H}_2$) atmospheres had a completely different physical appearance, as any sign of surface crystallization of iron-rich crystals was absent (Figure 4(b)). The SEM image of these glass-ceramics, along with their EDS elemental mapping, reveals a completely different microstructure where sodium aluminosilicate crystals with much larger grain size ($\sim 10 \mu\text{m}$ in size) (in comparison to those produced in air or N_2 atmospheres as shown in Figure 4(a)) can be seen along with some small flat shaped iron-rich crystals intermittently dispersed in the glass-ceramic matrix.

Contrary to the results of AF-series glass-ceramics, no gross surface crystal iron partitioning was observed in glass-ceramics with varying $\text{Na}_2\text{O}/\text{Fe}_2\text{O}_3$ ratio as a function of heating environment as is evident from Figures 4(c) and 4(d). The higher magnification SEM images (Figures 6(c) and 6(d)) revealed that the microstructure of the NF-2.5 glass-ceramics comprised of two different morphologies – thin plate-like iron-rich crystals embedded in distorted hexagonal-shaped nepheline crystals.

3.4 Impact of glass composition and heat treatment atmosphere on iron redox in glass-ceramics

Figures S6 – S8 present the Mössbauer spectra of glass-ceramics isothermally crystallized in three different atmospheres – air, inert (N₂) and reducing (N₂-H₂), while Table 6 presents the site populations of Fe²⁺ and Fe³⁺ obtained from these spectra. Details of their fitted hyperfine parameters CS, H (magnetic hyperfine field) and LW are presented in Tables S1 – S3. The Mössbauer spectra of all the glass-ceramics were fitted with two broadened Lorentzian doublets and two sextets. The fitted hyperfine parameters (CS, QS) are consistent with tetrahedrally-coordinated Fe³⁺ (Doublet 1) and octahedrally-coordinated Fe²⁺ (Doublet 2).^{25, 27, 39, 40} The hyperfine parameters (CS, LW and H) of the two sextets are consistent with the tetrahedral and octahedral sites of magnetite, Fe₃O₄.^{17, 58, 59}

The iron redox in glass-ceramics showed more compositional dependence than atmosphere dependence, as only minimal impact of heat treatment atmosphere (air/inert/reducing) was observed on Fe³⁺/ΣFe redox ratio, with the relative areas of the two doublets and two sextets changing little as a function of imposed *p*O₂. Differences between parameters obtained for AF-2.5 (Table S1) and AF-5 (Table S2) samples are also small, suggesting little change in iron redox chemistry between the two different iron contents studied. By far the greatest differences occur between the AF-2.5 and NF-2.5 (Table S3) glass-ceramics. The iron in NF-2.5 glass-ceramic is strongly partitioned into the crystalline Fe₃O₄ phase, and specifically the tetrahedral site (Sextet 1). This has occurred at the expense of the Fe³⁺ located in the glassy phase, as evidenced by the lower Doublet 1 area and higher Sextet 1 area by comparison with AF-2.5. On the other hand, the areas of the Fe²⁺ glassy phase (Doublet 2) and the Fe₃O₄ octahedral site (Sextet 2) change little from AF-2.5 to NF-2.5. The iron giving rise to Doublets 1 and 2 is most likely to be present in the residual glassy

phase, although hyperfine parameters are also broadly consistent with iron in nepheline.⁶⁰

The stability of the iron redox for a given sample, represented by the two doublets, further supports the possibility of at least some iron residing in nepheline, more likely Fe³⁺, since previous studies have shown that Fe³⁺ can incorporate into the structure of nepheline by substituting for Al³⁺, while there is no evidence for Fe²⁺ incorporating into the nepheline structure.^{23, 61, 62} It might reasonably be expected that a decrease in the Fe³⁺/Fe²⁺ ratio of the iron not present in the Fe₃O₄ magnetite phase (i.e. the iron giving rise to the two doublets) would occur with decreasing imposed pO_2 , such that Air > N₂ >> N₂-H₂. However, this does not occur and instead, the doublet redox remains stable. While the hyperfine parameters (CS, QS) of the two doublets are particularly consistent with the glassy phase, on the basis of the above, it is conceivable that this iron is distributed between glassy and nepheline / carnegieite phases.

3.5 Magnetic properties of glass-ceramics

The magnetic hysteresis loops of isothermally heat-treated samples with a maximum applied field (H_{max}) of 1.8 T, along with FORCs of samples isothermally heat-treated in air atmosphere are presented in Figure 7. FORCs of samples heat-treated in N₂ and N₂-H₂ atmospheres have been shown in Figure S9. Most of the samples with the same compositions show similar hysteresis behavior regardless of their different heat-treating atmospheres, which is consistent with the XRD and Mössbauer spectroscopy results. The AF-5 sample heat-treated in a reducing atmosphere (N₂-H₂) exhibits slightly higher magnetization than the other AF-5 samples as shown in Figure 7(c). Since this sample contains relatively higher amount of Fe in its composition, the reducing atmosphere is more likely to bring about Fe²⁺, which can result in magnetite crystallization. Magnetite (Fe₃O₄) as a ferrimagnetic phase leads to higher magnetization. A slight increase in magnetite sextet populations with

changing from oxidizing to reducing atmosphere was observed in the Mössbauer spectra as well. However, the results generally reveal that heating atmosphere does not significantly influence the crystallization of iron phases in the investigated samples. The highest magnetization values of AF-5 samples compared to the other two compositions suggest that higher iron concentrations in these samples lead to a higher fraction of magnetite. Nevertheless, NF-2.5 samples (Figure 7(e)) show higher magnetization than AF-2.5 samples (Figure 7(a)) despite having the same amount of Fe in both compositions. This is because of the higher availability of Fe ions in NF-2.5 samples, resulting in higher concentration of magnetite. In other words, since NF-2.5 samples crystallize less nepheline than AF-2.5 ones according to the XRD results, and it is known from previous studies that Fe tends to incorporate into nepheline structure,^{23, 61} there is more available Fe to crystallize as magnetite, which leads to higher magnetization in NF-2.5 samples. Mössbauer spectra also revealed higher populations of magnetite in NF-2.5 samples compared to AF-2.5 ones. The XRD results, however, show similar concentrations of magnetite within these samples, which is due to the fact that VSM measurements and Mössbauer spectroscopy are more sensitive to traces of magnetic phases (here magnetite) even if they are below the detection limit of XRD, as shown previously.²³ The different coercivities in the samples can originate from either different magnetic Fe-oxides (i.e., hematite and magnetite, where hematite typically has much higher coercivity) or different size distributions of magnetic grains.

FORC diagrams typically reveal additional information regarding the size and state of the magnetic grains. Different magnetic domain behaviors, which originate from the size of the magnetic grains, have a different signature in FORC diagrams. Any magnetic phase has its specific size threshold to transform from multi-domain state (larger grain size) to pseudo-single domain state (moderate grain sizes) to single-domain state (smaller grain size).⁶³ The

FORCs, shown in Figure S9, likewise demonstrate very similar behavior for the samples with the same composition regardless of heating atmosphere. AF-2.5 (Figure 7(b)) and AF-5 (Figure 7(d)) groups indicate a multi-domain behavior (more spread in the H_u axis) along with a single-domain behavior (elongated along the H_c axis), suggesting the presence of two distributions of a magnetic phase, likely magnetite, with distinct sizes. NF-2.5 samples (Figure 7(f)), on the contrary, show only weakly-interacting pseudo-single-domain (PSD) state, which is indicative of smaller grain size of magnetic phases than suggested by the results of the AF samples.

4. Discussion

4.1 Dependence of crystalline phase assemblage and microstructure on the heating atmosphere

The two most important results of the current study can be summarized as – (1) heating atmosphere does not exhibit significant impact on the overall crystalline phase assemblage (as measured by XRD) of the investigated glass-ceramics; (2) however, it does exhibit a substantial impact on their microstructure. The first part of results pertaining to insignificant change in crystalline phase assemblage as a function of heating environment can be explained on the basis of mechanisms that govern the reduction/oxidation (redox) reactions. It has been shown in literature that redox mechanisms are rate limited by diffusion of either O_2 or O^- ions at superliquidus temperatures, while they are rate limited by diffusion of divalent and monovalent cations at the redox front at lower temperature near the glass transition range.^{24, 64, 65} Moreover, near the glass transition range, the mobility of cations such as Na^+ would also depend on their concentration and whether they act as network modifiers or as charge compensators for AlO_4^- , FeO_4^- and BO_4^- .⁶⁵ In this study, the isothermal heat-treatments in different environments have been conducted at 700 °C. Being closer to the glass transition

range, the diffusivities of O₂ or O⁻ ions are expected to be low. Therefore, it is more likely that the redox reactions are being governed by cationic diffusion. This leads to minimal impact on the Fe³⁺/ΣFe ratio of glasses as a function of heating environment, thus resulting in insignificant change in the crystalline phase assemblage.

On the other hand, the dependence of the microstructure of the glass-ceramics on the heat treatment atmosphere (oxidizing vs. inert vs. reducing) is highly intriguing and raises several questions related to the mechanisms governing these reactions. The first question that needs to be answered is why did iron partition out of the glass structure in glass-ceramics AF-2.5 and AF-5, and form an iron oxide-rich crystalline layer on the surface of resultant glass-ceramic? As per the existing literature, this observation may be explained on the basis of outward diffusion of modifying ions in glasses.⁶⁶ According to Cook and Cooper,⁶⁷ the formation of an iron oxide-rich crystalline layer on the surface of glass-ceramics when heat treated in an air/oxidizing environment is governed by an outward cation diffusion process. When heated (crystallized) in air, the network modifying cations (in this case, alkali and Fe²⁺) diffuse from the interior of the glass to the free surface, where they subsequently react with environmental oxygen, to form an iron oxide-rich crystalline layer which covers the iron-depleted glass/glass-ceramic. Cook and Cooper⁶⁷ and Smith and Cooper⁶⁸ observed the formation of a two-phase, MgO-(Mg, Fe)₃O₄, crystalline layer on the surface of an iron-containing pyroxene-based alkaline-earth aluminosilicate glass. In the present study, we did not observe an association of sodium ions with an iron-rich crystalline layer on the surface of the glass-ceramic. This may be attributed to the slower diffusion of alkali cations in comparison to their divalent counterparts, as has been shown by Smedskjaer and Yue.⁶⁶ According to Smedskjaer and Yue,⁶⁶ the presence of iron (a transition metal) makes the silicate glass a polaron-type semiconductor (with consequent coupling and decoupling of

cation and anion fluxes). In such a scenario, the most rapid dissipation of the driving force (Gibbs energy associated with the redox reaction) involves the diffusion of fast-moving network modifying cations and faster-moving positively charged electron holes. It is the electron holes that dissipate the driving force, but to maintain charge neutrality their motion is charge-coupled with the motion of positively charged network modifying cations in the opposite direction. Since divalent cations (for example, Fe^{2+} , Ca^{2+} , Mg^{2+}) can carry more positive charge (and have smaller ionic radius)³ in comparison to monovalent alkali counterparts (Na^+ , K^+) to charge balance the flux of electron holes, divalent cations diffuse faster than alkali ions.^{66, 69} Further, Cook and Cooper⁶⁷ have suggested that the formation of an iron-rich crystalline layer on the surface of glass/glass-ceramic should not be confused with surface devitrification, as one would anticipate finding a silicate- or aluminosilicate-rich intergranular microstructure in this case; such has not been found experimentally. With regard to the formation of small flat-shaped iron-rich crystals intermittently dispersed in the matrices of glass-ceramics AF-2.5 and AF-5 crystallized in $\text{N}_2\text{-H}_2$ atmosphere, similar crystalline microstructure has been reported by Cook et al.⁶⁷ in iron-containing magnesium aluminosilicate glass-ceramics when heated in air. They had explained the formation of these crystals on the basis of internal oxidation of some Fe^{2+} within the glass. However, in our case, the presence of these iron-rich crystals in reducing atmosphere is still an open question and needs further experimental and theoretical analysis.⁶⁷

The second question is why we did not observe the formation of an iron-rich oxide layer on the surface of AF-2.5 and AF-5 glass-ceramics when heated in a reducing ($\text{N}_2\text{-H}_2$) atmosphere. This observation may be explained on the basis of inward diffusion of cations caused by the reduction of polyvalent ions (Fe^{3+} to Fe^{2+}) in the glass from the surface towards

³ The ionic radius of Na^+ is 116 pm while that of Fe^{2+} is 75 pm in high-spin state and 92 pm in low-spin state, as reported by Shannon [Ref. 68].

interior.⁶⁶ The mechanism of reduction depends on the H₂ pressure. At relatively high H₂ pressures, the permeation of H₂ into the glass dominates the reduction kinetics ($\text{H}_2 + 2(-\text{Si}-\text{O})^- + 2 \text{Fe}^{3+} \rightarrow 2 \text{Fe}^{2+} + 2(-\text{Si}-\text{OH}^+)$). However, when the H₂ pressure is low, holes are generated by the internal reduction of the polyvalent ion. These holes get filled by ionic oxygen at the surface since oxygen is released into the reducing atmosphere as H₂O. The outward flux (from the interior toward the surface) of electron holes from one polyvalent ion to another occurs, as described by Smedskjaer and Yue.⁷¹ To maintain charge neutrality, this process requires an inward diffusion (from the surface towards the interior) of mobile cations (Na⁺ and Fe²⁺, in this case). Since these network-modifying cations leave the glass surface without the diffusion of Al³⁺ and Si⁴⁺ ions, an aluminosilicate rich layer forms on the glass surface (instead of the iron-rich oxide layer).

While the concept of inward/outward diffusion of modifying cations partially explains the formation of iron-rich oxide layer in AF-2.5 and AF-5 glass-ceramics in air vs. reducing atmospheres, in our opinion, it is not universally applicable to all the glass systems containing iron or transition metal cations that exhibit change in redox chemistry with heating atmosphere. Our opinion is based on the fact that this concept does not explain the absence of iron-rich surface layer from NF-2.5 glass-ceramic when produced in an air or N₂ atmosphere. Similarly, we did not observe the formation of an iron-rich crystalline layer on the surface of glass-ceramics with composition 25 Na₂O – 20 Al₂O₃ – 5 Fe₂O₃ – 50 SiO₂ (mol.%) in our previous study.⁴ Also, there are several instances in the literature where no such iron oxide partitioning on the surface of glass-ceramics has been reported for iron-rich glass systems.^{72, 73}

In our opinion, in order to develop a holistic understanding of iron partitioning in certain glass-ceramics, while being absent in others, we also need to account for the kinetics of crystallization in glass melts. The glass NF-2.5 exhibits slow kinetics of crystallization (in comparison to AF-2.5) as is evident from crystalline phase evolution in this system (discussed above). Similarly, nuclear waste glasses are designed to exhibit low crystallization tendency. Therefore, in order to understand this complex phenomenon, the impact of chemical composition and environment on the redox behavior, structure, thermodynamics and kinetics of crystallization of silicate glasses and melts needs deeper consideration.

4.2 Implications of these results on the chemical durability of HLW glasses

The U.S. Department of Energy (DOE) is building a Tank Waste Treatment and Immobilization Plant (WTP) at Hanford site in Washington State to separately vitrify low activity waste (LAW) and high-level waste (HLW) in borosilicate glass at 1150 °C using Joule-heated ceramic melters (JHCM).⁷⁴ The current strategy is to pour the HLW glass melt into steel canisters, and transport them to a deep geological repository. During cooling of glass melt in steel canisters, the sodium and alumina-rich HLW glasses are prone to crystallization of nepheline which is likely to deteriorate the chemical durability of the final waste form.^{75, 76} Therefore, according to current HLW glass disposal requirements, nepheline precipitation must be either avoided, or be quantified and its impact on durability be controlled and predicted.⁷⁷ However, constraints, such as nepheline discriminator²² and optical basicity model,¹⁶ proposed to design HLW glass formulations with minimal tendency towards nepheline crystallization are not valid over broad composition space and also limit the potential for waste loading in the final waste form. Recently, a submixture model (SM) has been proposed by Vienna et. al.⁷⁸ which creates a pseudo-ternary diagram comprised of alkali and alkaline-earth oxides (Na₂O, Li₂O, K₂O, CaO and MgO) as one pseudo-

component; Al_2O_3 and Fe_2O_3 as the second; and SiO_2 , B_2O_3 and P_2O_5 as the third pseudo-component. This model has been reported to be a better predictor of nepheline formation than the previously proposed constraints. However, extensive data pertaining to nepheline crystallization in glasses over a broader compositional space is required to strengthen this sub-mixture model in order to design advanced glass formulations with increased waste loadings. The results from this study along with our previous studies.^{4, 7, 17, 23, 55, 79} will play a crucial role in further strengthening these predictive models.

From the viewpoint of impact of iron oxide partitioning and spinel (Fe_3O_4 in this case) formation on chemical durability of HLW glassy waste forms, it is noteworthy that formation of iron-rich layer on the surface of HLW glasses during centerline canister cooling (CCC) has been observed in the past.⁸⁰ While it has been generally accepted that spinel formation in the HLW glass melt are more problematic for melter operation and have minimal impact on the chemical durability of the waste form,^{76, 81} the same statement may or may not be valid for the iron oxide-rich layer formed on the surface of glassy waste forms depending on its volume concentration. The possibility of iron-oxide surface crystal formation depends greatly not only on the chemical composition of the HLW glass (as has been shown in the present study), but also on the pouring procedure into the steel canister. Most likely only hot glass surfaces exposed to ambient atmosphere for long durations would produce this layer. If melt is poured into the canister all at once, only the very top surface of the cylinder will be exposed to ambient atmosphere, resulting in a predicted very small fraction of iron oxides (<0.1 vol%). However, if more complex pours are used, such as has been studied previously,⁸² there may be more opportunities for higher concentration of iron oxide – rich crystalline layer formation on the surface of HLW glass.

Godon et al.⁸³ have shown that magnetite when in SON68 glass enhances glass alteration, first by the sorption of Si released from the glass onto magnetite surfaces, then by a second process that could be the precipitation of an iron silicate mineral or the transformation of magnetite into a more reactive phase like hematite or goethite. Similar results have also been reported by other researchers including Michelin et. al.⁸⁴ and Neill et. al.⁸⁵ Interestingly, in all the studies reported on this topic, iron or its oxides have been added externally in the aqueous corrosion medium. To the best of our knowledge, there does not exist any study describing the impact of an iron oxide rich layer formed on the surface of HLW glassy waste form on its chemical durability. However, based on the existing literature, we anticipate this iron-rich surface layer to have a detrimental impact on the chemical durability of the final waste form (depending on its concentration). Therefore, it is important to understand the chemical, structural and thermodynamic drivers governing the formation of this iron-rich layer on the surface of HLW glasses (in order to suppress its formation) during CCC and its impact on the long-term performance of the final waste form.

5. Summary and Conclusions

The crystallization behavior of boron and iron containing nepheline-based model high-level nuclear waste glasses has been studied as a function of glass chemistry and heating environment. The two most interesting results obtained from this study can be summarized as: heating atmosphere has (1) minimal impact on the overall crystalline phase assemblage of the studied glass-ceramics, and (2) substantial impact on their crystalline morphology and microstructure. While the first part of results pertaining to insignificant change in overall crystalline phase assemblage as a function of heating environment has been explained on the basis of low oxygen diffusion at temperatures near or above glass transition which govern the change in iron redox chemistry in glasses, the second part describing the formation or non-

Accepted Article

formation of iron-rich crystalline layer on the surface of glass-ceramics when heated in different atmospheres has been explained using the concept of inward/outward diffusion of modifying cations. However, it is worth mentioning that the phenomenon of formation or lack of formation of an iron-rich layer on the surface of glass-ceramics is highly complex and needs deeper consideration into the structure, thermodynamics and kinetics of crystallization of iron containing silicate glasses and melts. Further, the implications of crystalline phase assemblage and microstructure on the long-term performance of sodium and alumina-rich high-level nuclear waste glasses has been discussed.

Acknowledgement

This work was supported by funding provided by the U.S. Department of Energy (DOE), Office of River Protection, Waste Treatment & Immobilization Plant (WTP), through contract numbers DE-EM0003207 and DE-EM0002904, and U.S. DOE, Office of Nuclear Energy through the Nuclear Energy University Program under the award DE-NE0008597.

References

1. Buerger MJ. The Stuffed Derivatives of the Silica Structures. *Am Mineral.* 1954 July; 39: 600-614.
2. Donnay G, Schairer JF, Donnay JDH. Nepheline solid solutions. *Mineral Mag.* 1959; 32(245): 93-109.
3. Seifert FA, Mysen BO, Virgo D. Three-dimensional network structure of quenched melts (glass) in the systems $\text{SiO}_2\text{-NaAlO}_2$, $\text{SiO}_2\text{-CaAl}_2\text{O}_4$ and $\text{SiO}_2\text{-MgAl}_2\text{O}_4$. *Am Mineral.* 1982; 67(7-8): 696-717.
4. Shaharyar Y, Cheng JY, Han E, Maron A, Weaver J, Marcial J, et al. Elucidating the effect of iron speciation ($\text{Fe}^{2+}/\text{Fe}^{3+}$) on crystallization kinetics of sodium aluminosilicate glasses. *J Am Ceram Soc.* 2016; 99(7): 2306-2315.
5. Thompson JG, Withers RL, Whittaker AK, Traill RM, Fitzgerald JD. A Reinvestigation of Low-Carnegieite by XRD, NMR, and TEM. *J Solid State Chem.* 1993; 104(1): 59-73.
6. Duke DA, MacDowell JF, Karstetter BR. Crystallization and Chemical Strengthening of Nepheline Glass-Ceramics. *J Am Ceram Soc.* 1967; 50(2): 67-74.
7. Deshkar A, Marcial J, Southern SA, Kobera L, Bryce DL, McCloy JS, Goel A. Understanding the structural origin of crystalline phase transformations in nepheline (NaAlSiO_4) based glass-ceramics. *J Am Ceram Soc.* 2017; 100(7): 2859-2878.
8. Bowen NL. The binary system: $\text{Na}_2\text{Al}_2\text{Si}_2\text{O}_8$ (Nephelinite, Carnegieite) - $\text{CaAl}_2\text{Si}_2\text{O}_8$ (Anorthite). *Am J Sci.* 1912; 33: 551-573.
9. Kivlighn HD and Russak MA. Formation of Nepheline Glass-Ceramics Using Nb_2O_5 as a Nucleation Catalyt. *J Am Ceram Soc.* 1974; 57(9): 382-385.

- Accepted Article
10. Hamawy EMA and El-Meliegy EAM. Preparation of nepheline glass-ceramics for dental applications. *Mater Chem Phys*. 2008; 112(2): 432-435.
 11. Wang MC, Wu NC, Hon MH. Preparation of Nepheline Glass-Ceramics and their Application as Dental Porcelain. *Mater Chem Phys*. 1994; 37(4): 370-375.
 12. Holand W, Beall G. *Glass-Ceramic Technology*. Hoboken, NJ: The American Ceramic Society and Wiley; 2002. Applications of glass-ceramics; p. 252-353.
 13. Ellison AJ, Moore LA, Werner TL. Opaque Colored Glass-Ceramics Comprising Nepheline Crystal Phases. U.S. Patent 20,150,284,288. 2015.
 14. Beall GH, Comte M, Dejneka MJ, Marques P, Pradeau P, Smith C. Ion-Exchange in Glass-Ceramics. *Front. Mater*. 2016; 3: 41.
 15. Goel A, McCloy JS, Fox KM, Leslie CJ, Riley BJ, Rodriguez CP, et al. Structural analysis of some sodium and alumina rich high-level nuclear waste glasses. *J Non-Cryst Solids*. 2012; 358(3): 674-679.
 16. McCloy JS, Schweiger MJ, Rodriguez CP, Vienna JD. Nepheline Crystallization in Nuclear Waste Glasses: Progress Toward Acceptance of High-Alumina Formulations. *Int J Appl Glass Sci*. 2011; 2(3): 201-214.
 17. McCloy J, Washton N, Gassman P, Marcial J, Weaver J, Kukkadapu R. Nepheline crystallization in boron-rich aluminosilicate glasses as investigated by multi-nuclear NMR, Raman, & Mossbauer spectroscopies. *J Non-Cryst Solids*. 2015; 409: 149-165.
 18. Matyáš J, Vienna JD, Peeler DK, Fox KM, Herman CC, Kruger AA. Road map for development of crystal-tolerant high level waste glasses. Richland, WA: Pacific Northwest National Laboratory; 2014. 19 p. PNNL-23363.
 19. Rodriguez CP, McCloy JS, Schweiger MJ, Crum JV, Winschell A. Optical basicity and nepheline crystallization in high alumina glasses. Richland, WA: Pacific Northwest National Laboratory; 2011. 92 p. PNNL-20184.
 20. Matyáš J, Gervasio V, Sannoh SE, Kruger AA. Predictive modeling of crystal accumulation in high-level waste glass melters processing radioactive waste. *J Nucl Mater*. 2017; 495(Supplement C): 322-331.
 21. Edwards M, Matyáš J, Crum J. Real-time monitoring of crystal accumulation in the high-level waste glass melters using an electrical conductivity method. *Int J Appl Glass Sci*. 2018; 9(1): 42-51.
 22. Li H, Vienna JD, Hrma P, Smith DE, Schweiger MJ. Nepheline precipitation in high-level waste glasses: Compositional effects and impact on the waste form acceptability. In: Gray WJ, Triay IR, eds. *Scientific Basis for Nuclear Waste Management XX*, Materials Research Society Proceedings, vol. 465. Boston, MA: Materials Research Society; 1997: p. 261-268
 23. Ahmadzadeh M, Marcial J, McCloy J. Crystallization of iron-containing sodium aluminosilicate glasses in the NaAlSiO₄-NaFeSiO₄ join. *J Geophys Res Solid Earth*. 2017; 122(4): 2504-2524.
 24. Mysen B, Richet P. *Silicate glasses and melts: properties and structure*, Vol. 10. Amsterdam, The Netherlands: Elsevier; 2005.
 25. Mysen BO. The structural behavior of ferric and ferrous iron in aluminosilicate glass near meta-aluminosilicate joins. *Geochim Cosmochim Acta*. 2006; 70(9): 2337-2353.
 26. Magnien V, Neuville DR, Cormier L, Mysen BO, Briois V, Belin S, et al. Kinetics of iron oxidation in silicate melts: a preliminary XANES study. *Chem Geol*. 2004; 213(1-3): 253-263.
 27. Cochain B, Neuville DR, Henderson GS, McCammon CA, Pinet O, Richet P. Effects of the Iron Content and Redox State on the Structure of Sodium Borosilicate Glasses: A Raman, Mössbauer and Boron K-Edge XANES Spectroscopy Study. *J Am Ceram Soc*. 2012; 95(3): 962-971.
 28. Virgo D, Mysen BO. The structural state of iron in oxidized vs. reduced glasses at 1 atm – A ⁵⁷Fe Mossbauer study. *Phys Chem Miner*. 1985; 12(2): 65-76.
 29. Kress VC, Carmichael ISE. The compressibility of silicate liquids containing Fe₂O₃ and the effect of composition, temperature, oxygen fugacity and pressure on their redox states. *Contrib Miner Petrol*. 1991; 108(1): 82-92.
 30. Calas G, Petiau J. Coordination of iron in oxide glasses through high-resolution K-edge spectra: Information from the pre-edge. *Solid State Commun*. 1983; 48(7): 625-629.
 31. Rossano S, Ramos AY, Delaye JM. Environment of ferrous iron in CaFeSi₂O₆ glass: contributions of EXAFS and molecular dynamics. *J Non-Cryst Solids*. 2000; 273(1-3): 48-52.

32. Wang Z, Cooney TF, Sharma SK. High temperature structural investigation of $\text{Na}_2\text{O}\cdot 0.5\text{Fe}_2\text{O}_3\cdot 3\text{SiO}_2$ and $\text{Na}_2\text{O}\cdot \text{FeO}\cdot 3\text{SiO}_2$ melts and glasses. *Contrib Mineral Petrol.* 1993; 115(1): 112-122.
33. Keppler H. Crystal-field spectra and geochemistry of transition-metal ions in silicate melts and glasses. *Am Mineral.* 1992; 77(1-2): 62-75.
34. Theodore MB, Karl ES. Thermochemical Modeling of Oxide Glasses. *J Am Ceram Soc* 2004; 85(12): 2887-2894.
35. Qian MX, Li LY, Li H, Strachan DM. Partitioning of gadolinium and its induced phase separation in sodium-aluminoborosilicate glasses. *J Non-Crystal Solids.* 2004; 333(1): 1-15.
36. Brehault A, Patil D, Kamat H, Youngman RE, Thirion LM, Mauro JC, Corkhill CL, McCloy JS, Goel A. Compositional dependence of solubility/retention of molybdenum oxides in aluminoborosilicate-based model nuclear waste glasses. *J Phys Chem B* 2018; 122(5): 1714-29.
37. Roberts AP, Pike CR, Verosub KL. First-order reversal curve diagrams: A new tool for characterizing the magnetic properties of natural samples. *J Geophys Res Solid Earth.* 2000; 105(B12): 28461-28475.
38. Harrison RJ, Feinberg JM. FORCinel: An improved algorithm for calculating first-order reversal curve distributions using locally weighted regression smoothing. *Geochem Geophys Geosys.* 2008; 9(5) Q05016.
39. Bingham PA, Parker JM, Searle T, Williams JM, Fyles K. Redox and clustering of iron in silicate glasses. *J Non-Cryst Solids.* 1999; 253(1-3): 203-209.
40. Burns RG. Mineral Mössbauer spectroscopy: Correlations between chemical shift and quadrupole splitting parameters. *Hyperfine Interact.* 1994; 91(1): 739-745.
41. Dyar MD, Agresti DG, Schaefer MW, Grant CA, Sklute EC. Mössbauer spectroscopy of earth and planetary materials. *Annu Rev Earth Planet Sci.* 2006; 34(1): 83-125.
42. Duffy JA. Redox equilibria in glass. *J Non-Cryst Solids* 1996; 196: 45-50.
43. Schreiber HD, Kochanowski BK, Schreiber CW, Morgan AB, Coolbaugh MT, Dunlap TG. Compositional dependence of redox equilibria in sodium – silicate glasses. *J Non-Cryst Solids* 1994; 177: 340-46.
44. Duffy JA, Ingram MD. An interpretation of glass chemistry in terms of the optical basicity concept. *J Non-Cryst Solids* 1976; 21(3): 373-410.
45. McCloy JS, Vienna, JD. Glass composition constraint recommendations for use in life-cycle mission modeling. Richland, WA: Pacific Northwest National Laboratory; 2010. 54 p. PNNL-19372
46. Dvorinchenko IN, Matsenko SV. Structure of glasses in the $\text{Na}_2\text{O} - \text{Fe}_2\text{O}_3 - \text{B}_2\text{O}_3 - \text{SiO}_2$ system. *Glass Ceram.* 2000; 57(1): 11-13.
47. Williams KFE, Johnson CE, Thomas MF. Mössbauer spectroscopy measurement of iron oxidation states in float composition silica glasses. *J Non-Cryst Solids.* 1998; 226(1-2): 19-23.
48. Jayasuriya KD, O'Neill HS, Berry AJ, Campbell SJ. A Mössbauer study of the oxidation state of Fe in silicate melts. *Am Mineral.* 2004; 89(11-12): 1597-1609.
49. Mekki A, Holland C, McConville CF, Salim M. An XPS study of iron sodium silicate glass surfaces. *J. Non-Cryst Solids* 1996; 208(3): 267-76.
50. Sorensen PM, Pind M, Yue YZ, Rawlings RD, Boccaccini AR, Nielsen ER. Effect of the redox state and concentration of iron on the crystallization behavior of iron-rich aluminosilicate glasses. *J Non-Crystal Solids.* 2005; 351(14-15): 1246-1253.
51. Klein LC, Fasano BV, Wu JM. Viscous flow behavior of four iron-containing silicates with alumina, effects of composition and oxidation condition. *J Geophys Res Solid Earth.* 1983; 88(S02): A880-A886.
52. Jensen M, Zhang L, Yue Y. Probing iron redox state in multicomponent glasses by XPS. *Chem Geol.* 2012; 322: 145-150.
53. Sun KH, Huggins ML. Energy additivity in oxygen-containing crystals and glasses. *J Phys Chem.* 1947; 51(2): 438-443.
54. Li H, Hirma P, Vienna JD, Qian M, Su Y, Smith DE. Effects of Al_2O_3 , B_2O_3 , Na_2O , and SiO_2 on nepheline formation in borosilicate glasses: chemical and physical correlations. *J Non-Cryst Solids.* 2003; 331(1-3): 202-216.

55. Marcial J, Crum J, Neill O, McCloy J. Nepheline Structural and Chemical Dependence on Melt Composition. *Am Mineral*. 2016; 101(2): 266-276.
56. Abbott RN. KAlSiO_4 stuffed derivatives of tridymite - phase-relationships. *Am Mineral*. 1984; 69(5-6): 449-457.
57. Martin MI, Andreola F, Barbieri L, Bondioli F, Lancellotti I, Rincon JM, et al. Crystallisation and microstructure of nepheline-forsterite glass-ceramics. *Ceram Int*. 2013; 39(3): 2955-2966.
58. Romero M, Rincón JM, Mûsik S, Kozhukharov V. Mössbauer effect and X-ray distribution function analysis in complex $\text{Na}_2\text{O}-\text{CaO}-\text{ZnO}-\text{Fe}_2\text{O}_3-\text{Al}_2\text{O}_3-\text{SiO}_2$ glasses and glass-ceramics. *Mater Res Bull*. 1999; 34(7): 1107-1115.
59. Sharma K, Singh S, Prajapat CL, Bhattacharya S, Jagannath, et al. Preparation and study of magnetic properties of silico phosphate glass and glass-ceramics having iron and zinc oxide. *J Magn Magn Mater*. 2009; 321(22): 3821-3828.
60. Wu Y, Wu X, Tu B. Phase relations of the nepheline-kalsilite system: X-ray diffraction and Mössbauer spectroscopy. *J Alloys Compd*. 2017; 712: 613-617.
61. Onuma K, Iwai T, Yagi K. Nepheline-"Iron Nepheline" Solid Solutions. *J Fac Sci. Hokkaido Univ Ser 4 Geol Mineral*. 1972; 15(1-2): 179-190.
62. Onuma K, Yoshikawa K. Nepheline solid solutions in the system $\text{Na}_2\text{O}-\text{Fe}_2\text{O}_3-\text{Al}_2\text{O}_3-\text{SiO}_2$. *J Jpn Assoc Mineral Petrol Econ Geol*. 1972; 67: 395-401.
63. Dunlop DJ, Özdemir Ö. *Rock Magnetism: Fundamentals and Frontiers*. Cambridge University Press: Cambridge; 1997.
64. Schreiber HD, Kozak SJ, Merkel RC, Balazs GB, Jones PW. Redox equilibria and kinetics of iron in a borosilicate glass-forming melt. *J Non-Cryst Solids*. 1986; 84(1): 186-195.
65. Magnien V, Neuville DR, Cormier L, Roux J, Hazemann JL, de Ligny D, et al. Kinetics and mechanisms of iron redox reactions in silicate melts: The effects of temperature and alkali cations. *Geochim Cosmochim Acta*. 2008; 72(8): 2157-2168.
66. Smedskjaer MM, Yue YZ. Inward and Outward Diffusion of Modifying Ions and its Impact on the Properties of Glasses and Glass-Ceramics. *Int J Appl Glass Sci*. 2011; 2(2): 117-128.
67. Cook GB, Cooper RF, Wu T. Chemical diffusion and crystalline nucleation during oxidation of ferrous iron-bearing magnesium aluminosilicate glass. *J Non-Cryst Solids*. 1990; 120(1-3): 207-222.
68. Smith DR, Cooper RF. Dynamic oxidation of a Fe^{2+} -bearing calcium-magnesium-aluminosilicate glass: the effect of molecular structure on chemical diffusion and reaction morphology. *J Non-Cryst Solids*. 2000; 278(1-3): 145-163.
69. Shannon RD. Revised effective ionic radii and systematic studies of interatomic distances in halides and chalcogenides. *Acta Cryst A*. 1976; 32(5): 751-67.
70. Wu T, Kohlstedt DL. Rutherford backscattering spectroscopy study of the kinetics of oxidation of $(\text{Mg,Fe})_2\text{SiO}_4$. *J Am Ceram Soc*. 1988; 71(7): 540-545.
71. Smedskjaer MM, Yue YZ. Inward cationic diffusion in glass. *J. Non-Cryst. Solids* 2009; 355 (14-15): 908-12.
72. Karamanov A, Pisciella P, Cantalini C, Pelino M. Influence of $\text{Fe}^{3+}/\text{Fe}^{2+}$ Ratio on the Crystallization of Iron-Rich Glasses Made with Industrial Wastes. *J Am Ceram Soc*. 2000; 83(12): 3153-3157.
73. Karamanov A, Pelino M. Crystallization phenomena in iron-rich glasses. *J Non-Cryst Solids* 2001; 281 (1-3): 139-51.
74. U.S. Department of Energy. Hanford tank waste retrieval, treatment, and disposition framework. Washington D.C.; 2013. Download from: <http://energy.gov/downloads/hanfordtank-waste-retrieval-treatment-and-disposition-framework>.
75. Kim DS, Peeler DK, Hrma P. Effect of crystallization on the chemical durability of simulated nuclear waste glasses. In: Jain V, Palmer R, eds. *Ceramic Transactions Vol. 61, Environmental and Waste Management Technologies in the Ceramic and Nuclear Industries*. The American Ceramic Society, Westerville, OH; 1995: 177-185.
76. Riley BJ, Rosario JA, Hrma PR. Impact of HLW Glass Crystallinity on the PCT Response. Richland, WA: Pacific Northwest National Laboratory; 2001. 107 p. PNNL-13491.

77. ASTM. C 1285-08. Standard Test Methods for Determining Chemical Durability of Nuclear Hazardous, and Mixed Waste Glasses and Multiphase Glass Ceramics: The Product Consistency Test (PCT). West Conshohocken, PA: ASTM International; 2008.
78. Vienna JD, Kroll JO, Hrma PR, Lang JB, Crum JV. Submixture model to predict nepheline precipitation in waste glasses. *Int J Appl Glass Sci.* 2017; 8(2): 143-157.
79. Marcial J, Ahmadzadeh M, McCloy JS. Effect of Li, Fe, and B addition on the crystallization behavior of sodium aluminosilicate glasses as analogues for Hanford high level waste glasses. *MRS Adv.* 2017; 2(10): 549-555.
80. McCloy JS, Rodriguez C, Windisch C, Leslie C, Schweiger MJ, Riley BR, et al. Alkali/Alkaline-Earth Content Effects on Properties of High-Alumina Nuclear Waste Glasses. In: Fox KM, Hoffman E, Manjooan N, Pickrell G, eds. *Ceramic Transactions, 222, Advances in Materials Science for Environmental and Nuclear Technology.* John Wiley & Sons, Hoboken, NJ; 2010:p. 63-76.
81. Jantzen CM, Bickford DF. Leaching of Devitrified Glass Containing Simulated SRP Nuclear Waste. *MRS Proceedings.* 1984; 44: 135.
82. Amoroso J. Computer modeling of high-level waste glass temperatures within DWPF canisters during pouring and cool down. United States, Department of Energy; 2011. 69 p. SRNL-STI-2011-00546.
83. Godon N, Gin S, Rebiscoul D, Frugier P. SON68 Glass Alteration Enhanced by Magnetite. *Procedia Earth Planet Sci.* 2013; 7(Supplement C): 300-303.
84. Michelin A, Burger E, Leroy E, Foy E, Neff D, Benzerara K, et al. Effect of iron metal and siderite on the durability of simulated archeological glassy material. *Corros Sci.* 2013; 76(Supplement C): 403-414.
85. Neill L, Gin S, Ducasse T, Echave T, Fournier M, Jollivet P, et al. Various effects of magnetite on international simple glass (ISG) dissolution: implications for the long-term durability of nuclear glasses. *npj Mater Degrad.* 2017; 1(1): 1-11.

Figure Captions

Figure 1. Fitted Mössbauer spectra for glasses (a) AF-2.5, (b) AF-5 and (c) NF-2.5. Doublets have been labelled as D1 and D2.

Figure 2. DSC scans of glasses at 10 °C/min (N₂ atmosphere): (a) AF-0, (b) AF-2.5, (c) AF-5 and (d) NF-2.5

Figure 3. X-ray diffractograms of glasses heat treated non-isothermally at 10 °C/min and air quenched at different temperatures: (a) AF-0, (b) AF-2.5, (c) AF-5 and (d) NF-2.5

Figure 4. EDS elemental maps of isothermally heat-treated samples at 700 °C (a) AF-5 in air; (b) AF-5 in N₂-H₂; (c) NF-2.5 in air and (d) NF-2.5 in N₂-H₂. (Microstructural images were taken in secondary electron imaging mode). The areas marked “Fe-rich” in (a), (b) and (c) denote the iron-rich regions found on the surface of samples, while the areas marked “NP” in (a) and (b) represent the microstructure of nepheline phase.

Figure 5. A piece of AF-2.5 glass-ceramic (fractured to show the core as well as surface) obtained by isothermally heating the glass in air atmosphere at 700 °C for 1 hour, showing golden-brown layer on surface and a dark brown halo in the core.

Figure 6. Secondary electron (SE) images of glass samples crystallized (a) AF-2.5 in air, (b) AF-5 in air, (c) NF-2.5 in air and (d) NF-2.5 in N₂-H₂ atmospheres. The areas marked “Fe-rich” in (a), (b) and (c) denote the iron-rich regions found on the surface of samples, while the areas marked “NP” in (a) and (b) represent nepheline crystals.

Figure 7. Magnetic hysteresis loops up to 1.8 T of isothermally heat-treated glass-ceramics: (a) AF-2.5, (c) AF-5 and (e) NF-2.5. FORC diagrams of samples isothermally heat-treated in air: (b) AF-2.5 700 °C Air, (d) AF-5 700 °C Air and (f) NF-2.5 700 °C Air. In FORC diagrams, single domain (SD) and multi-domain (MD) regions have been labelled. In NF-2.5 sample, pseudo-single domain (PSD) behavior was observed. Smoothing factors (SF) for FORC diagrams were as follows: SF = 6 for AF-2.5, SF = 5 for AF-5 and SF = 3 for NF-2.5 samples.

Table 1. Batched vs. experimental compositions. "--" indicates that compositional analysis was not conducted on these samples since they crystallized

| | | Compositions | | | | | | |
|--------------------------------|---------------------|--------------|--------|-------|--------|---------|-------|--------|
| | | AF-0 | AF-2.5 | AF-5 | NF-2.5 | AF-6.25 | NF-5 | BF-2.5 |
| Na ₂ O | mol.% (batched) | 25.00 | 25.00 | 25.00 | 22.50 | 25.00 | 20.00 | 25.00 |
| | wt.% (batched) | 22.17 | 21.72 | 21.29 | 19.28 | 21.08 | 16.58 | 21.48 |
| | wt.% (experimental) | 21.0 | 20.7 | 20.4 | 18.8 | -- | -- | -- |
| Fe ₂ O ₃ | mol.% (batched) | 0.00 | 2.50 | 5.00 | 2.50 | 6.25 | 5.00 | 2.50 |
| | wt.% (batched) | 0.00 | 5.60 | 10.97 | 5.52 | 13.58 | 10.68 | 5.53 |
| | wt.% (experimental) | 0.00 | 5.85 | 11.7 | 5.81 | -- | -- | -- |
| Al ₂ O ₃ | mol.% (batched) | 20.00 | 17.50 | 15.00 | 20.00 | 13.75 | 20.00 | 20.00 |
| | wt.% (batched) | 29.18 | 25.02 | 21.02 | 28.19 | 19.08 | 27.27 | 28.27 |
| | wt.% (experimental) | 31.6 | 26.5 | 22.9 | 30.1 | -- | -- | -- |
| B ₂ O ₃ | mol.% (batched) | 10.00 | 10.00 | 10.00 | 10.00 | 10.00 | 10.00 | 7.50 |
| | wt.% (batched) | 9.96 | 9.76 | 9.57 | 9.63 | 9.47 | 9.31 | 7.24 |
| | wt.% (experimental) | 8.73 | 8.30 | 8.16 | 8.47 | -- | -- | -- |
| SiO ₂ | mol.% (batched) | 45.00 | 45.00 | 45.00 | 45.00 | 45.00 | 45.00 | 45.00 |
| | wt.% (batched) | 38.69 | 37.90 | 37.15 | 37.38 | 36.79 | 36.16 | 37.48 |
| | wt.% (experimental) | 38.8 | 37.50 | 37.50 | 37.2 | -- | -- | -- |

Table 2. Mössbauer spectroscopy results of glasses - fitted hyperfine parameters of AF-2.5, AF-5 and NF-2.5

| Sample | Doublet 1 (Fe ³⁺) | | | Doublet 2 (Fe ²⁺) | | | Area (Doublet 1 / Total) = Fe ³⁺ /ΣFe (±0.02) | Fit reduced χ ² |
|--------|---------------------------------------|---------------------------------------|---------------------------------------|---------------------------------------|---------------------------------------|---------------------------------------|---|----------------------------------|
| | CS (±0.02) / mm s ⁻¹ | QS (±0.02) / mm s ⁻¹ | LW (±0.02) / mm s ⁻¹ | CS (±0.02) / mm s ⁻¹ | QS (±0.02) / mm s ⁻¹ | LW (±0.02) / mm s ⁻¹ | | |
| AF-2.5 | 0.25 | 0.92 | 0.37 | 0.96 | 1.90 | 0.42 | 0.719 | 0.597 |
| AF-5 | 0.24 | 0.96 | 0.30 | 1.00 | 1.93 | 0.31 | 0.781 | 0.682 |
| NF-2.5 | 0.26 | 0.98 | 0.35 | 1.03 | 1.98 | 0.41 | 0.641 | 0.749 |

Table 3. Thermal parameters (in °C) – T_g, T_c, T_{p1}, T_{p2}, T_m obtained from DSC-Heating curve

| Glass | T _g | T _c | T _{p1} | T _{p2} | T _m |
|---------|----------------|----------------|-----------------|-----------------|----------------|
| AF-0 | 567.81 ± 4.4 | 720.18 ± 2.5 | 770.1 | -- | 1168.4 ± 2.9 |
| AF- 2.5 | 531.50 ± 4.9 | 615.23 ± 1.1 | 636.1 ± 1.7 | 671.9 ± 3.5 | 892.1 ± 3.5 |
| AF- 5 | 507.80 ± 2.1 | 658.90 ± 1.5 | 713.4 ± 2.8 | -- | 870.4 ± 11.0 |
| NF- 2.5 | -- | 613.50 ± 1.1 | 641.1 ± 1.6 | 733.3 ± 1.3 | 962.2 ± 12.7 |

Table 4. Summary of qualitative XRD phase analysis of non-isothermal heat-treatments on glasses. A = amorphous; U = unidentified phase; NP = nepheline; CG = orthorhombic carnegieite and M = magnetite. In case of multiple phases detected at one temperature, the first one written in order is the major phase

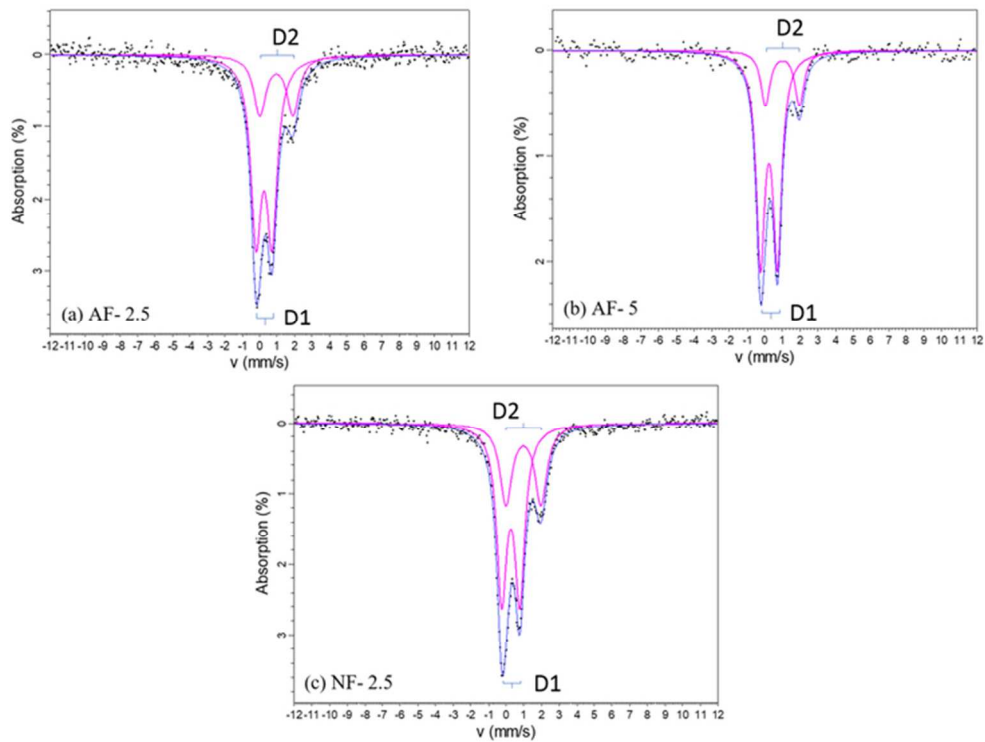
| | Temperature (°C) | | | | | | | | | | |
|--------|------------------|--------|-------------|-------------|-------------|--------|--------|------------|------------|--------|------|
| | 580 | 600 | 640 | 660 | 680 | 700 | 780 | 820 | 840 | 920 | 1020 |
| AF-0 | A | A | A | A | A | A | A | A | U | U + NP | NP |
| AF-2.5 | U | U + NP | U + NP + M | NP + M | NP + M | NP + M | -- | -- | -- | -- | -- |
| AF-5 | A | CG | CG + NP + M | NP + CG + M | NP + CG + M | NP + M | -- | -- | -- | -- | -- |
| NF-2.5 | A | A | A | A | U | U | U + NP | U + NP + M | NP + U + M | -- | -- |

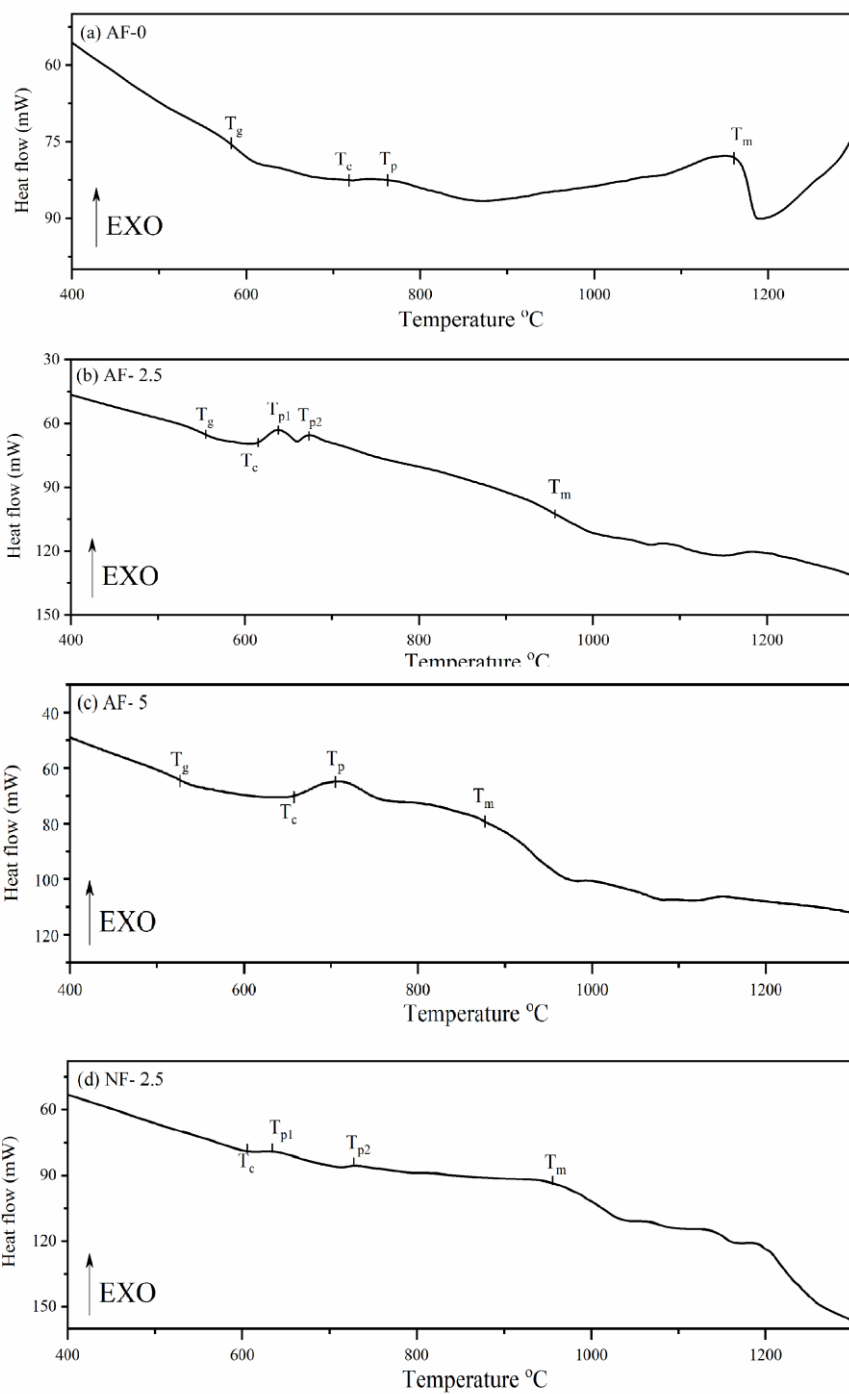
Table 5. Results of Rietveld refinement analysis on isothermally heat-treated glasses at 700 °C for 1 hour

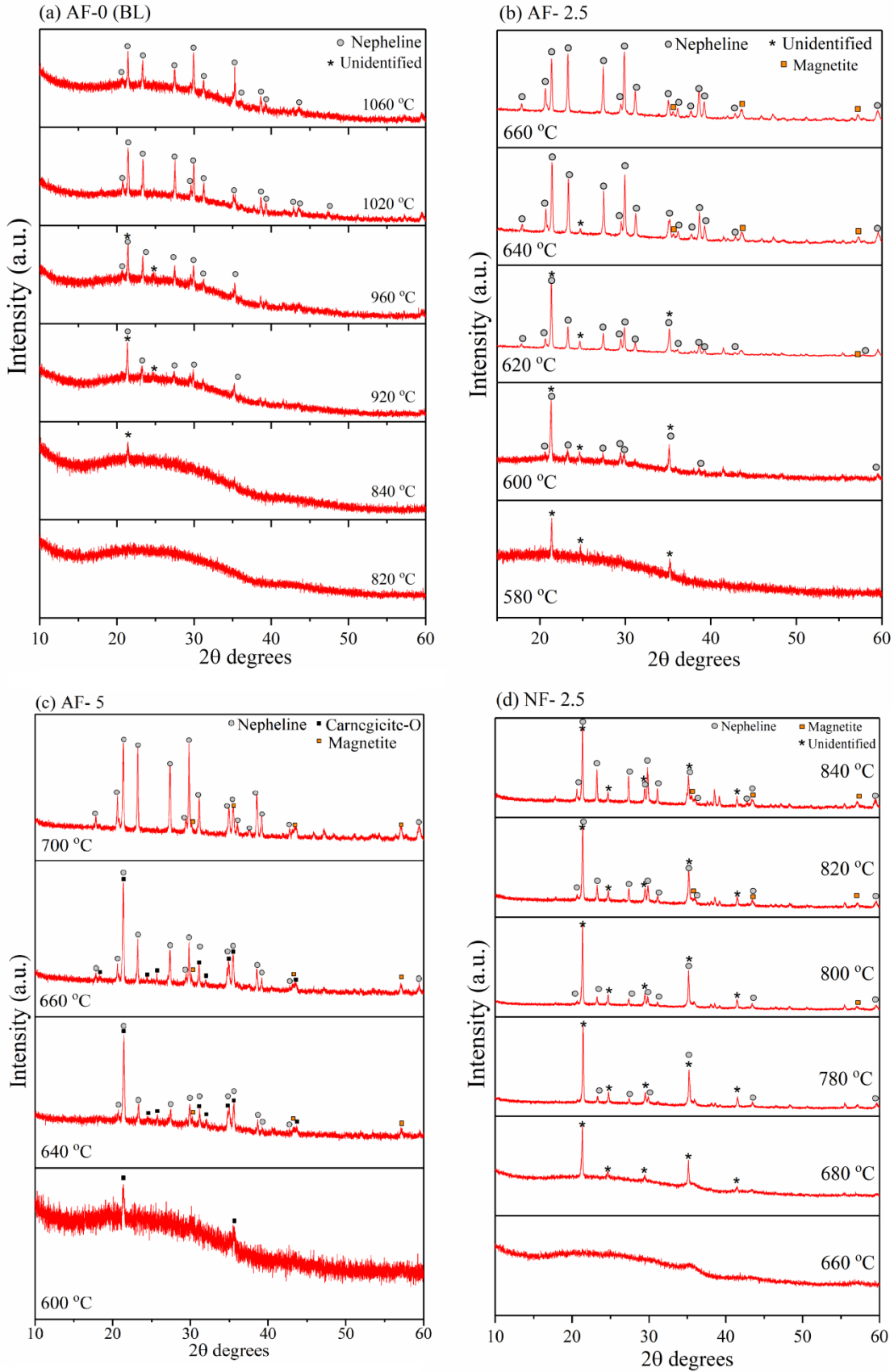
| Sample | Proportion (wt. %) | | | | |
|--------------------------------|--------------------|-------------|-----------|----------|-----------|
| AF-0 | Nepheline | Carnegieite | Magnetite | Hematite | Amorphous |
| Air | 34.6 | 9.7 | -- | -- | 55.7 |
| | | | | | |
| AF-2.5 | Nepheline | Carnegieite | Magnetite | Hematite | Amorphous |
| Air | 33.3 | 0.0 | 0.2 | 0.7 | 65.8 |
| N ₂ | 32.9 | 0.0 | 0.2 | 0.6 | 66.3 |
| N ₂ -H ₂ | 30.7 | 0.0 | 0.2 | 0.8 | 68.4 |
| | | | | | |
| AF-5 | Nepheline | Carnegieite | Magnetite | Hematite | Amorphous |
| Air | 30.6 | 0.7 | 0.1 | 1.4 | 67.1 |
| N ₂ | 26.7 | 0.4 | 0.1 | 0.8 | 72.0 |
| N ₂ -H ₂ | 28.2 | 0.2 | 0.0 | 1.5 | 70.1 |
| | | | | | |
| NF-2.5 | Nepheline | Carnegieite | Magnetite | Hematite | Amorphous |
| Air | 24.5 | 0.9 | 0.002 | 1.1 | 73.3 |
| N ₂ | 19.0 | 5.8 | 0.003 | 0.6 | 74.3 |
| N ₂ -H ₂ | 20.3 | 3.6 | 0.0 | 1.5 | 74.5 |

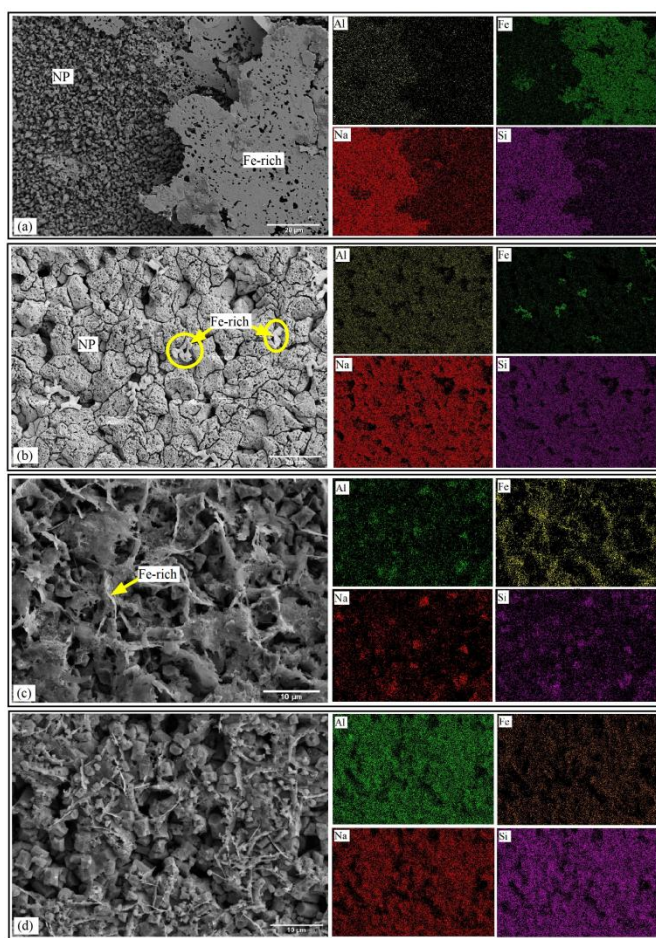
Table 6. Site populations of Fe²⁺ and Fe³⁺ sites as obtained from Mössbauer spectroscopy of isothermally heat-treated glasses at 700 °C for 1 hour

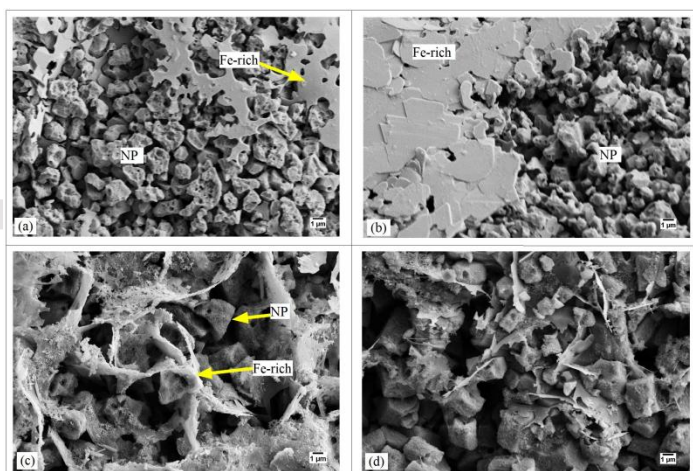
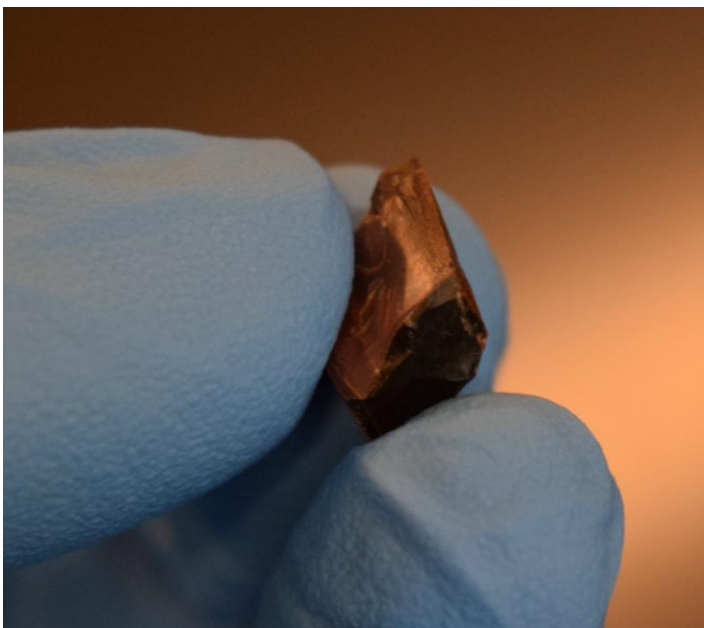
| | Site Population (area%) | | | |
|--------------------------------|-------------------------------|-------------------------------|------------------------------|------------------------------|
| AF-2.5 | Doublet 1 (Fe ³⁺) | Doublet 2 (Fe ²⁺) | Sextet 1 (Fe ³⁺) | Sextet 2 (Fe ²⁺) |
| Air | 45.1 | 13.8 | 27.5 | 13.7 |
| N ₂ | 44.2 | 15.5 | 25.6 | 14.7 |
| N ₂ -H ₂ | 44.9 | 11.9 | 28.3 | 14.9 |
| | | | | |
| AF-5 | Doublet 1 (Fe ³⁺) | Doublet 2 (Fe ²⁺) | Sextet 1 (Fe ³⁺) | Sextet 2 (Fe ²⁺) |
| Air | 40.5 | 8.5 | 33.3 | 17.8 |
| N ₂ | 44.3 | 7.1 | 31.0 | 17.6 |
| N ₂ -H ₂ | 34.9 | 13.2 | 36.3 | 15.6 |
| | | | | |
| NF-2.5 | Doublet 1 (Fe ³⁺) | Doublet 2 (Fe ²⁺) | Sextet 1 (Fe ³⁺) | Sextet 2 (Fe ²⁺) |
| Air | 10.5 | 9.8 | 60.0 | 19.5 |
| N ₂ | 9.6 | 12.1 | 63.2 | 15.1 |
| N ₂ -H ₂ | 8.9 | 6.3 | 68.3 | 16.5 |

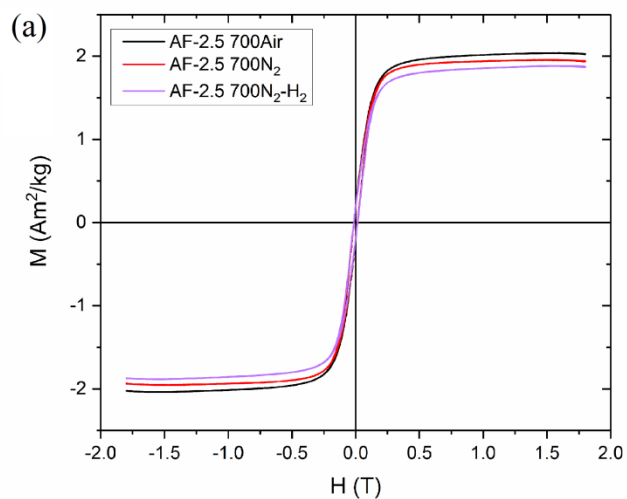




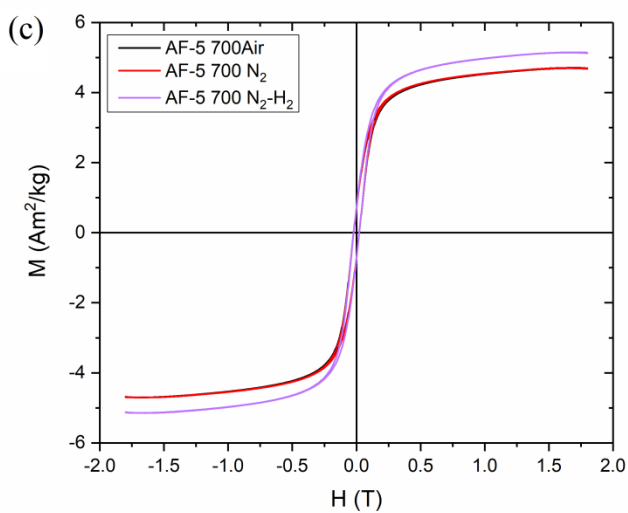
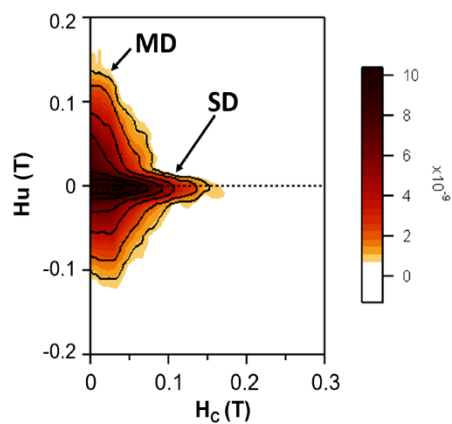




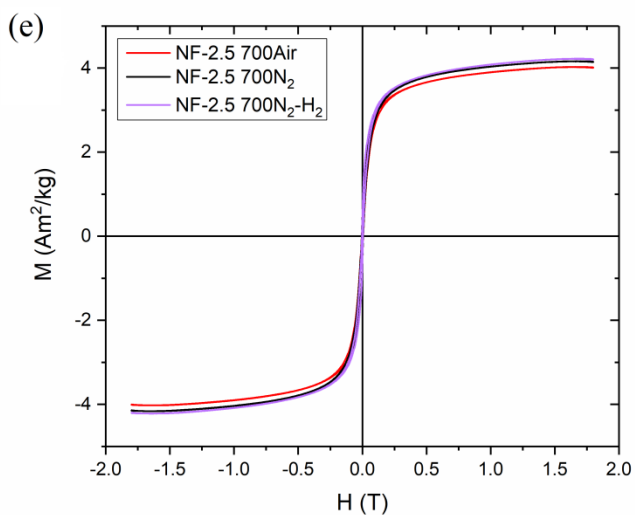
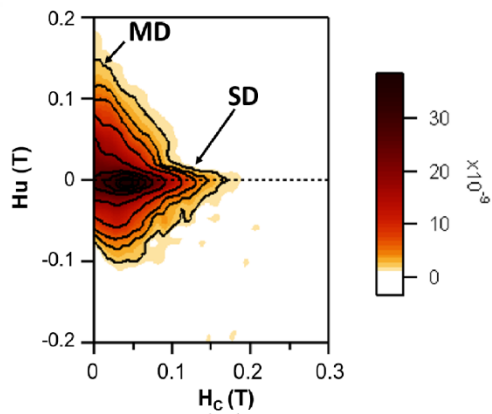




(b) AF-2.5 700 °C Air: FORC



(d) AF-5 700 °C Air: FORC



(f) NF-2.5 700 °C Air: FORC

